Decoding the spermatogonial stem cell niche under physiological and recovery conditions in adult mice and humans

Jin, Cheng; Wang, Zhipeng; Li, Pengyu; Tang, Jielin; Jiao, Tao; Li, Yiran

Published in:
Science Advances

DOI:
10.1126/sciadv.abq3173

Publication date:
2023

DEVELOPMENTAL BIOLOGY

Decoding the spermatogonial stem cell niche under physiological and recovery conditions in adult mice and humans

Cheng Jin[1,2,3]†, Zhipeng Wang[1]†, Pengyu Li[1], Jielin Tang[1], Tao Jiao[1], Yiran Li[1], Jinhuan Ou[1], Dingfeng Zou[1], Mengzhen Li[1], Xinyu Mang[1], Jun Liu[1], Yanni Ma[1,4], Xiaolong Wu[5], Jie Shi[5], Shitao Chen[6], Manman He[1], Yan Lu[1], Ning Zhang[4,7], Shiying Miao[1], Fei Sun[5], Linfang Wang[1], Kai Li[1]*, Jia Yu[1,4]*, Wei Song[1]*

The intricate interaction between spermatogonial stem cell (SSC) and testicular niche is essential for maintaining SSC homeostasis; however, this interaction remains largely uncharacterized. In this study, to characterize the underlying signaling pathways and related paracrine factors, we delineated the intercellular interactions between SSC and niche cell in both adult mice and humans under physiological conditions and dissected the niche-derived regulation of SSC maintenance under recovery conditions, thus uncovering the essential role of C-C motif chemokine ligand 24 and insulin-like growth factor binding protein 7 in SSC maintenance. We also established the clinical relevance of specific paracrine factors in human fertility. Collectively, our work on decoding the adult SSC niche serves as a valuable reference for future studies on the aetiology, diagnosis, and treatment of male infertility.

INTRODUCTION

In mammals, spermatogonial stem cells (SSCs), a heterogeneous subset of undifferentiated spermatogonia (uSPG), constitute the initial cell population for spermatogenesis. SSC reside in a microenvironment where they differentiate and develop into fertile sperms, playing a critical role in spermatogenesis. This niche is composed of different types of somatic cells that interact with germline cells, which are essential for the maintenance of uSPG homeostasis, expansion of differentiating SPG (dSPG), and recovery after testicular injury (*1*–*3*). Many studies have attempted to identify and functionally explore niche-derived paracrine factors and related signaling pathways that regulate SSC behavior. Stem cell factor secreted by Sertoli cells (SER) influences type A SPG expansion (*4*), glial cell line–derived neurotrophic factor (GDNF) secreted by SER and peritubular myoid cells (PMCs) promotes SSC self-renewal (*5*), and additional factors such as fibroblast growth factor 2 (FGF2) and retinoic acid (RA) are also required for SSC self-renewal or differentiation (*6*, *7*). However, a comprehensive delineation of the physical and functional connections between SSC and its niche remains elusive.

In recent years, single-cell RNA sequencing (scRNA-seq) has enabled a systematic understanding of the intercellular regulation of mammalian spermatogenesis (*8*–*15*). However, because of the complex cell composition and complicated feedback regulation between niche and germ cells at different stages of differentiation in the testes (*16*), it is challenging to distinguish the signals that specifically regulate the function of SSC in vivo. In addition, the rapid transition from SSC to downstream progeny substantially narrows the window for capturing specific interactions between SSC and surrounding niche cells, which compromises the accuracy of results (*17*–*19*). A $Kit^{W/Wv}$ (W) mouse model has been established to eliminate non-SSC germ lines while maintaining competent SSC that can be fully proliferated and passaged in vitro (*20*, *21*). In addition, the testicular microenvironment is believed to be functionally intact in W mice because of their ability to produce normal progeny after correcting the proto-oncogene receptor tyrosine kinase (KIT) mutation with autografts or transplantation of normal donor SSC (*21*–*24*). Thus, the W mouse model could serve as an appropriate model for in vivo study of SSC, which not only excludes the majority of feedback regulation between niche and differentiated germ cells at different stages but also narrows down the range of niche-derived signals that can regulate the maintenance or differentiation of SSC. Theoretically, both maintenance and differentiation-promoting factors may be up-regulated in W mice. Nevertheless, previous studies have shown that niche cells in W mice were responsive to progressive SSC loss by up-regulating the expression of paracrine factors critical for SSC maintenance (*17*), which is further enhanced in the process of germline regeneration (*1*), indicating that W mice are a suitable model for in vivo study of SSC maintenance.

In this study, we used single-cell transcriptome analysis to decode the intercellular interaction between SSC and their niche

[1]Department of Biochemistry and Molecular Biology, State Key Laboratory of Common Mechanism Research for Major Diseases, Institute of Basic Medical Sciences, Chinese Academy of Medical Sciences, School of Basic Medicine, Peking Union Medical College, Beijing 100005, China. [2]Affiliated Foshan Maternity and Child Healthcare Hospital, Southern Medical University (Foshan Maternity & Child Healthcare Hospital), Foshan 528000, China. [3]Department of Developmental Biology, School of Basic Medical Sciences, Southern Medical University, Guangzhou, Guangdong, China. [4]Center for Stem Cell and Regeneration Medicine, Chinese Academy of Medical Sciences & Peking Union Medical College (PUMC), Chengdu 610052, China. [5]Institute of Reproductive Medicine, School of Medicine, Nantong University, Nantong 226001, China. [6]International Peace Maternity and Child Health Hospital, Shanghai Key Laboratory for Reproductive Medicine, School of Medicine, Shanghai Jiaotong University, Shanghai 200030, China. [7]Medical Research Council Protein Phosphorylation and Ubiquitylation Unit (MRC-PPU), School of Life Sciences, University of Dundee, Dundee DD1 5EH, UK.
*Corresponding author. Email: songwei@ibms.pumc.edu.cn (W.S.); j-yu@ibms.pumc.edu.cn (J.Y.); likai@ibms.pumc.edu.cn (K.L.)
†These authors contributed equally to this work.

cells under physiological conditions in both adult mice and humans and highlight the niche-derived regulation for SSC maintenance using W and wild-type (WT) mice models under recovery conditions. We further validated the speculated signaling pathways and uncovered paracrine factors essential for SSC maintenance, represented by CCL24 and insulin-like growth factor binding protein 7 (IGFBP7), in vitro and in vivo. Last, we confirmed the relationship between dysregulation of these paracrine factors, as part of the SSC niche functional connection, with human infertility.

RESULTS

Intercellular interactions between niche cell and SSC in adult mice and humans

We performed scRNA-seq on whole testicular cells derived from adult C57BL/6J mice (WT) using the 10x Genomics Chromium platform (Fig. 1A). In total, 14,840 high-quality single-cell transcriptomes were clustered on the basis of uniform manifold approximation and projection (UMAP). Using previously established cell type–specific markers, we distinguished between individual germ lines and niche cell subpopulations (*8*, *9*). Niche cells included SER (*Sox9*), Leydig cells (LEY; *Hsd3b1*), PMCs (*Acta2*), macrophages (MAC; *Adgre1*), innate lymphoid cells (LYM; *Ccl5*), mesenchymal cells (MES; *Tcf21*), and endothelial cells (END; *Vwf*). Sperm lines comprised SPG, including uSPG (*Zbtb16*), dSPG (*Kit*), spermatocytes (SPC; *Sycp3*), and spermatids (SPT; *Zp3r* and *Tnp1*) (Fig. 1B and fig. S1, A and B). SPG were then reclustered to identify the SSC using classic stem cell markers, such as *Gfra1*, *Ret*, *Etv5*, and *Eomes* (Fig. 1C and fig. S1C) (*8*–*15*). Furthermore, gene set enrichment analysis (GSEA) revealed that various aspects of functionality, including cytokine binding, extracellular matrix binding, cell adhesion molecules, growth factor binding, and cytokine receptor interaction, were specifically enriched in SSC (Fig. 1D).

To decipher the ligand-receptor (L-R) interaction between SSC and niche cell under physiological conditions (*16*), we assigned the ligands or receptors identified in each individual cell type with reference to the established databases (CellPhoneDB and FANTOM5) incorporating immune-relevant cytokines, chemokines, coinhibitors, costimulators, and their receptors. Niche cell–derived ligands that interact with SSC-derived receptors and their respective L-R pairs were identified (Fig. 1, E and F, and table S1). Two hundred L-R pairs were common between different niche cell types and SSC, and a number of SSC and niche cell–specific L-R pairs were likely to participate in cell type–specific regulation (fig. S1, D and E). We further characterized L-R interactions between niche cell and SSC in humans under physiological conditions using the adult human testicular scRNA-seq dataset (GSE124263) (*12*). The identified cell types were SER/END, LEY, PMC, MAC, MES, uSPG, dSPG, SPC, and SPT (fig. S2, A and B). The SSC population was identified from uSPG using accepted markers such as *FGFR3*, *UTF1*, *ID4*, *PIWIL4*, and *TSPAN33* (fig. S2, C and D). We found ligands or receptors expressed in the respective cell types and L-R pairs between niche cell and SSC (Fig. 1, G and H, and table S2), among which the L-R pairs shared by all niche cell types were distinguished from those specific for individual niche cell types (fig. S2, E and F). In addition, we identified L-R pairs that were conserved between adult mice and humans (Fig. 1I and table S2). Further analysis revealed that adherence junctions and tight junctions were the main cell-cell connections between SSC and SER in mice and humans (Fig. 1J), suggesting the potential role of this direct contact in regulating SSC. Overall, we established a comprehensive catalog of intercellular interactions, including L-R pairs and cell-cell connections, between niche cell and SSC under physiological conditions in mice and humans.

Niche-SSC interactions during SSC recovery

In adult mammals, SSC give rise to all progeny during spermatogenesis; thus, they are critical for recovery from disruptions. To understand the role of niche-SSC interactions, scRNA-seq was performed on whole testicular cells from adult C57BL/6J mice (WT), W mice, and *W* mice after 3 or 5 days of busulfan treatment (W3 and W5) (Fig. 1A). Fewer zinc finger and BTB domain containing 16 positive ($ZBTB16^{+}$) uSPG remained in the seminiferous tubules of W, W3, and W5 mice as compared to those of WT mice (fig. S3, A and B). Different cell types were identified in each sample using the corresponding cell markers (fig. S3C). Germ cells comprised most of the cells in WT mice (87% SPT, 5.6% SPC, and 3% SPG), whereas the proportion of each niche cell type was relatively smaller (4.4% somatic cells; Fig. 2A and fig. S3D). However, this composition greatly shifted toward somatic cells in samples collected from W, W3, and W5 mice (96.9% somatic cells and 3.1% SPG in W mice), thus enabling us to study the contribution of SSC niche to SSC recovery by comparing the signatures of niche cells among all four samples (Fig. 2A and fig. S3D). After filtering SPC and SPT, the combined dataset was reclustered, and niche cells of all four samples were used for intercellular interaction analysis under recovery conditions (Fig. 2B and fig. S3E). Cells from WT, W, W3, and W5 mice were batched together according to the corresponding cell type, suggesting consistency in the transcriptome based on the cell type between samples.

Paracrine factors secreted by the respective niche cells were annotated on the basis of the UniProt Knowledgebase (Fig. 2C and table S3). Gene ontology (GO) term enrichment analysis showed that the biological processes were enriched in stemness maintenance, proliferation, and cytokine- or growth factor–mediated signaling in W, W3, and W5 mice, suggesting the potential support of niche-SSC interconnection for SSC maintenance (fig. S4A). Consistently, pseudotime analysis of all SPG from WT, W, W3, and W5 mice showed that the SPG from W, W3, and W5 mice were located at the starting point of the developmental trajectory with high expression of SSC markers (fig. S4, B and C). These results suggested that, under recovery conditions, responsive niche cells secrete factors that promote SSC maintenance and stemness via intercellular regulation in W, W3, and W5 mice. Thus, we speculated that paracrine factors shared by WT, W, W3, and W5 mice per niche cell type participate in potential paracrine regulation of SSC maintenance under physiological conditions. All L-R interactions between niche cells and SSC in WT mice were classified into four categories, including WT mice–specific; common to WT, W, W3, and W5 mice; common to WT mice and humans; or common to WT, W, W3, and W5 mice and humans (Fig. 2D and table S4). We highlighted L-R interactions common to WT, W, W3, and W5 mice as candidate L-R interactions regulating SSC maintenance. Except for LYM, most of the L-R pairs between niche cell and SSC in WT mice were common to W, W3, and W5 mice and conserved in humans (Fig. 2E). L-R pairs specifically identified in the human dataset that might be involved in human-specific regulation of SPG are also listed in table S4.

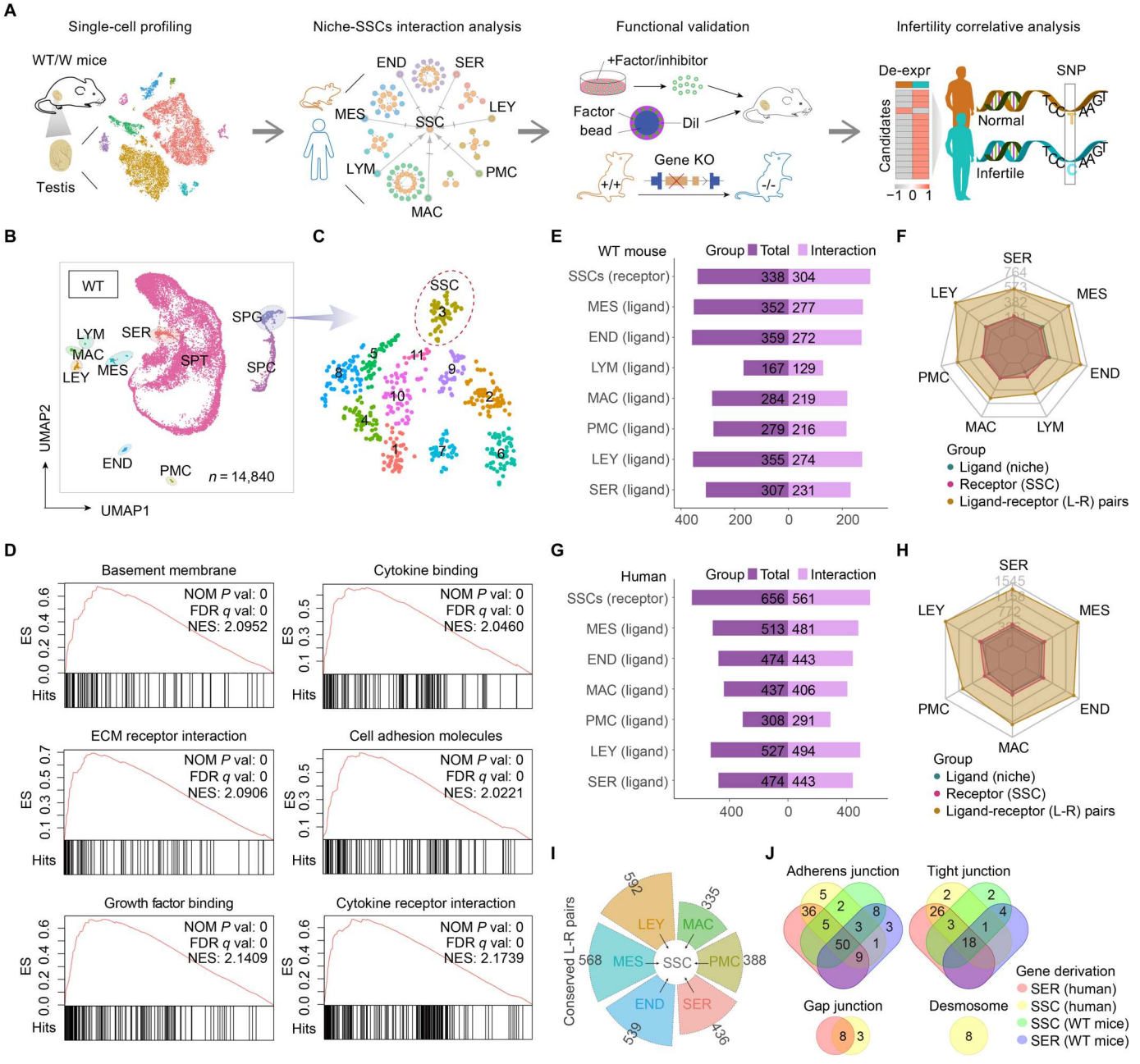

Fig. 1. Cellular interactions between SSC and niche cells in adult mice and humans. (**A**) Schematic illustration of the research workflow. WT, wild-type C57BL/6J mice; W, *Kit*$^{W/Wv}$ mice. SNP, single-nucleotide polymorphism. (**B**) Uniform manifold approximation and projection (UMAP) plots of testicular cells in adult WT mice colored by cell type. SER, Sertoli cells; LEY, Leydig cells; PMC, peritubular myoid cells; MAC, macrophage cells; LYM, innate lymphoid cells; MES, mesenchymal cells; END, endothelial cells; SPG, spermatogonia; SPC, spermatocytes; SPT, spermatids. (**C**) Recluster of SPG in WT mice coloured by subcluster. (**D**) Gene set enrichment analysis (GSEA) of biological process enriched in spermatogonial stem cells (SSC). NOM, nominal; FDR, false discovery rate; ES, enrichment score; NES, normalized ES. (**E**) The number of total ligands and ligands interacting with receptors in SSC in each somatic cell type in adult WT mouse testis. (**F**) Radar chart showing the number of ligand-receptor (L-R) pairs between each somatic cell type and SSC as well as the involved ligands and receptors in adult WT mouse testis. (**G**) The number of total ligands and ligands interacting with receptors in SSC in each somatic cell type in healthy adult human testis (GSE124263). (**H**) Radar chart showing the number of L-R pairs between each somatic cell type and SSC as well as the involved ligands and receptors in healthy adult human testis. (**I**) The conserved L-R pairs in each somatic cell type and SSC between adult mice and humans. (**J**) Venn diagram showing the similarities of cell-cell interaction between SER and SSC in adult mice and humans.

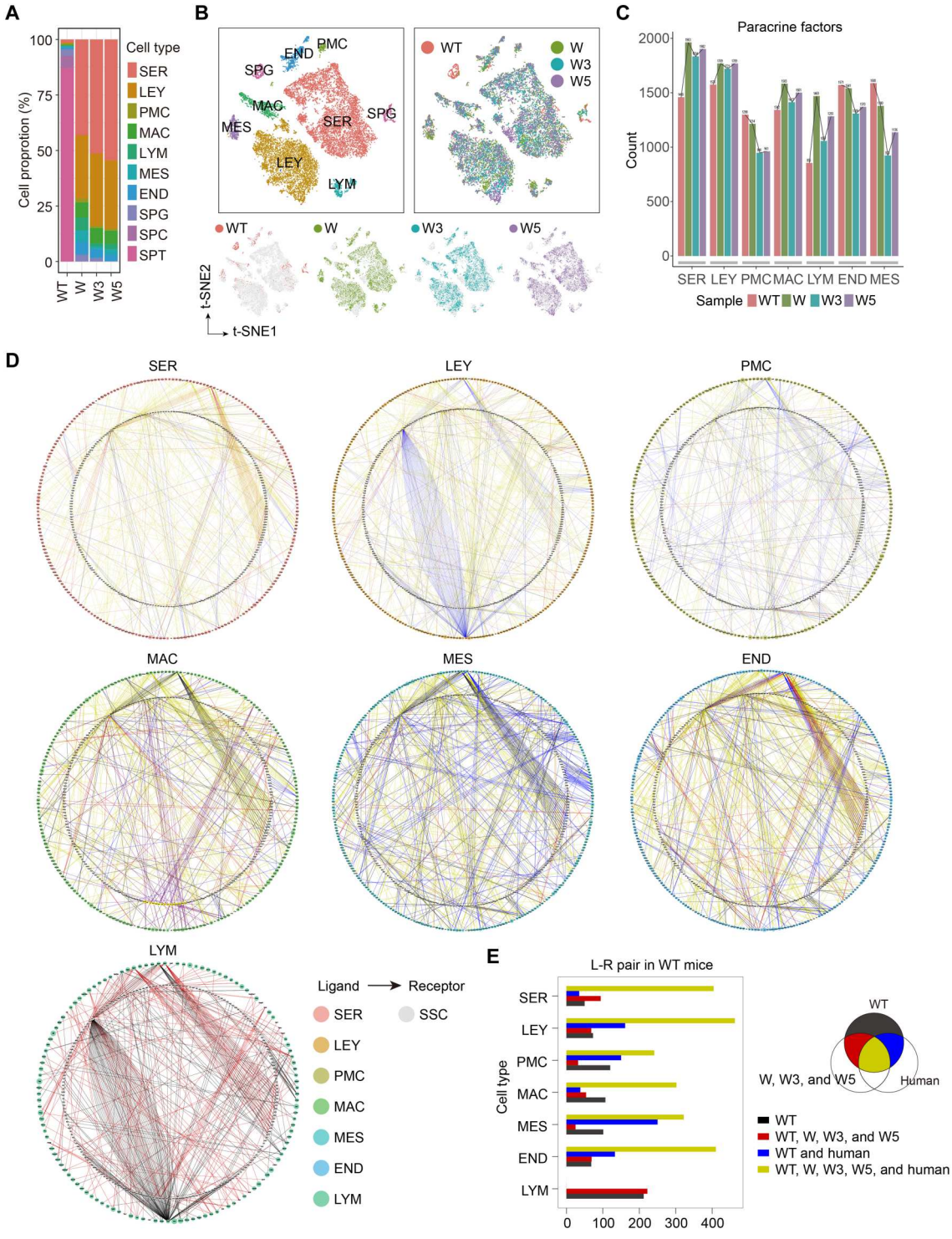

Fig. 2. L-R pairs between SSC and niche cells under physiological or recovery conditions. (**A**) Proportion of different cell types (%) in each sample. (**B**) t-distributed stochastic neighbor embedding (t-SNE) plots of niche cells and SPG from adult WT, W, W3, and W5 mice colored by cell type or samples. W3 and W5, *Kit*$^{W/Wv}$ mice 3 or 5 days after busulfan treatment. (**C**) Number of paracrine factors in each somatic cell type per sample. (**D**) L-R pairs between each somatic cell type and SSC in WT mouse testis. The edges were colored red for common L-R pairs in WT, W, W3, and W5 mice; blue for L-R pairs conserved in WT mice and humans; and green for L-R pairs common in WT, W, W3, W5, and human. (**E**) The number of L-R pairs with different attributions in the testes of WT C57BL/6J mice.

Niche-derived signaling pathways in regulating SSC maintenance

To explore the niche-derived signaling pathways regulating SSC, paracrine factors derived from different niche cell types of WT, W, W3, and W5 mice and membrane proteins in SSC of WT mice were categorized and subjected to Kyoto Encyclopedia of Genes and Genomes (KEGG) analysis (Fig. 3A and table S3). Potential signaling pathways under physiological (WT) or recovery (W, W3, and W5) conditions were characterized (Fig. 3B). The signaling pathways shared by WT, W, W3, and W5 mice in the same niche cell type (condition no. 1) and SSC-derived signaling pathways (condition no. 2) were identified as putative signaling pathways regulating SSC maintenance or differentiation. Seven signaling pathways met both conditions no. 1 and no. 2, including the phosphatidylinositol 3-kinase (PI3K)–Akt, resistance to audiogenic seizures (Ras), RAS-related protein 1 (Rap1), mitogen-activated protein kinase (MAPK), and Hippo signaling pathways, extracellular matrix (ECM)–receptor interactions, as well as cell adhesion molecules (Fig. 3B), in line

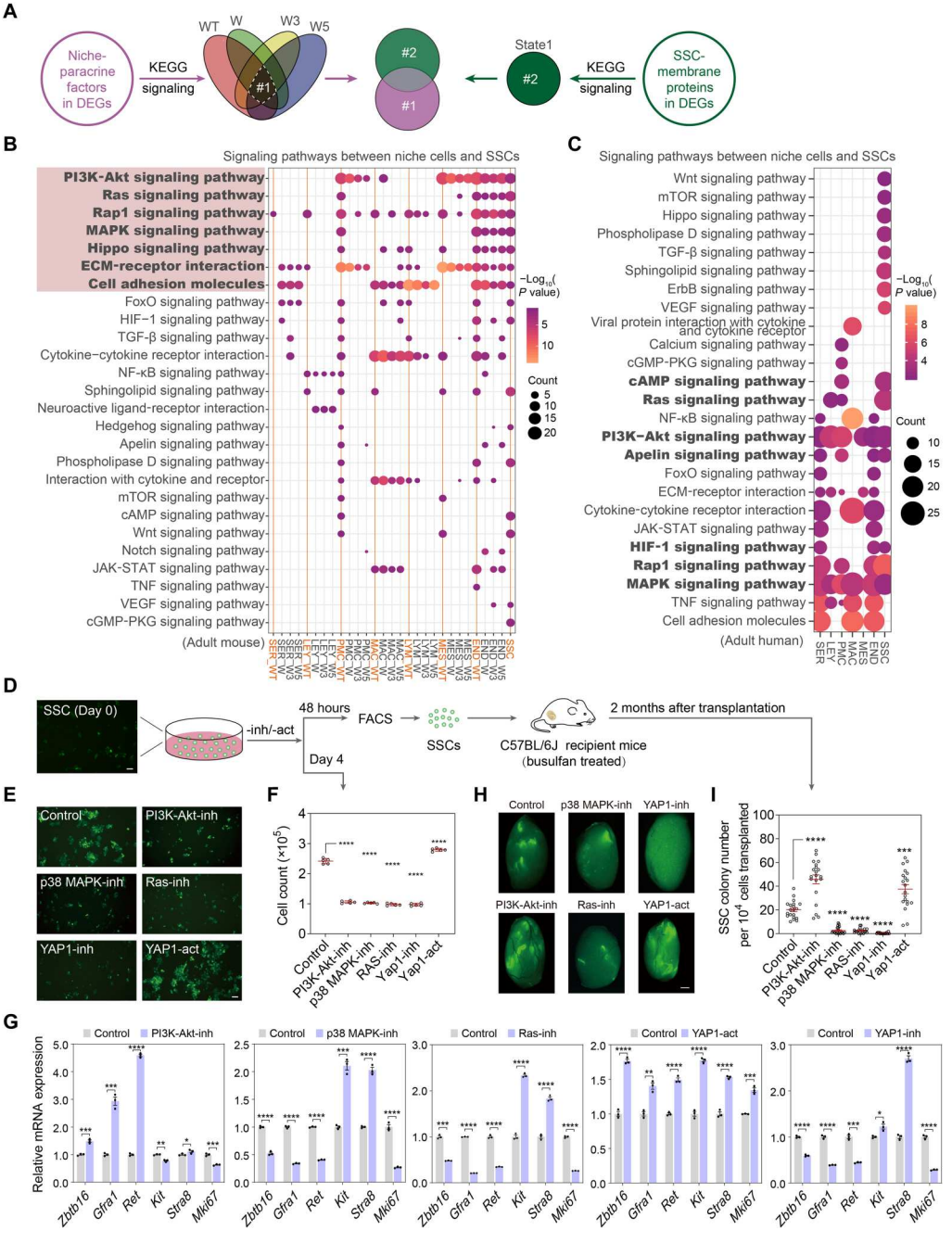

Fig. 3. Niche-derived signaling pathways in regulating SSC maintenance in adult mice and humans. (**A**) Strategy for identifying common niche-derived signaling pathways. DEGs, differentially expressed genes; KEGG, Kyoto Encyclopedia of Genes and Genomes. (**B**) Overview of the signaling pathways encompassing niche-derived paracrine factors and SSC-derived membrane proteins in adult mice. The pathways matching "#1" and "#2" datasets were highlighted with a pink box. PI3K-Akt, phosphatidylinositol 3-kinase–Akt; MAPK, mitogen-activated protein kinase; ECM, extracellular matrix; HIF-1, hypoxia-inducible factor 1; TGF-β, transforming growth factor–β; NF-κB, nuclear factor κB; cAMP, cyclic adenosine 3′,5′-monophosphate; JAK-STAT, Janus kinase–signal transducer and activator of transcription; TNF, tumor necrosis factor; VEGF, vascular endothelial growth factor; cGMP-PKG, cyclic guanosine 3′,5′-monophosphate–cGMP-dependent protein kinase. mTOR, mammalian (mechanistic) target of rapamycin (**C**) Overview of the signaling pathways encompassing niche-derived paracrine factors and SSC-derived membrane proteins identified in adult humans. (**D**) Strategy for functional validation of candidate signaling pathways. FACS, fluorescence-activated cell sorting. (**E**) SSC colony formed by in vitro–cultured enhanced green fluorescent protein–positive (EGFP$^+$) SSC after 4 days of coculture with corresponding signaling pathway inhibitor (-inh) or activator (-act) (scale bar, 50 μm). (**F**) The cell number of in vitro–cultured EGFP$^+$ SSC after 4 days of coculture with corresponding signaling pathway inhibitor or activator (n = 5). Values represent means ± SEM, and P values were obtained using one-way analysis of variance (ANOVA) followed by Tukey test (****P < 0.0001). (**G**) Quantitative reverse transcription polymerase chain reaction (RT-PCR) analysis (n = 3) of the stemness and differentiation markers in cultured SSC treated with corresponding signaling pathway inhibitors or activators. (**H**) Recipient testes 2 months after SSC transplantation (scale bar, 1 mm). Values represent means ± SEM, and P values were obtained using two-tailed t tests (*P < 0.05; **P < 0.01; ***P < 0.001; ****P < 0.0001). (**I**) The number of EGFP$^+$ SSC colonies formed in the recipient testes for each group (n = 20). Values represent means ± SEM, and P values were obtained using one-way ANOVA followed by Tukey test (***P < 0.001; ****P < 0.0001).

with the current understanding of these signaling pathways in regulating SSC proliferation, self-renewal, stemness, and/or survival (*25*–*30*). Using a similar strategy, we identified signaling pathways that potentially regulate SSC in adult humans (Fig. 3C). The PI3K-Akt, Ras, Rap1, and MAPK signaling pathways were also enriched in both human SSC and niche cells, indicating their potential role in regulating human SSC. Overall, we provide systematic insights into niche-derived paracrine regulation of SSC via signaling pathways under physiological or recovery conditions in mice and humans.

Next, we determined the activity of candidate signaling pathways regulating SSC in vivo. Immunofluorescence staining for phospho-p44/42 MAPK (Erk1/2) showed strong signals in GATA binding protein 4 positive ($GATA4^+$) SER and protein lin-28 homolog A positive ($LIN28A^+$) uSPG in seminiferous tubules (fig. S5A). In contrast, phospho-p38 MAPK showed strong signals in $LIN28A^+$ uSPG but not in $GATA4^+$ SER, indicating the specific function of p38 MAPK signaling in uSPG (fig. S5B). Yes-associated protein 1 (YAP1) showed positive signals in the nuclei of a subset of $LIN28A^+$ uSPG (fig. S5C), and phospho-PI3K p85/p55 showed positive signals in both $GATA4^+$ SER and $LIN28A^+$ uSPG (fig. S5D). These results indicate the activation of these signaling pathways in uSPG population. Bioinformatic analysis of differentially expressed niche-derived paracrine factors indicated their involvement in extracellular signal–regulated kinase (ERK), c-Jun N-terminal kinase (JNK), and p38 MAPK signaling pathways (fig. S5E). For example, angiopoietin 2 (ANGPT2) combined with FGF receptor 1 (FGFR1) was involved in the ERK and JNK signaling pathways, and transforming growth factor beta 1 (TGFB1) combined with TGFB receptor 2 (TGFBR2) was involved in the p38 signaling pathway.

We further dissected the functional contributions of putative signaling pathways to the regulation of SSC maintenance using chemical inhibitors/activators (table S7). Because both Jnk and Erk MAPKs are downstream of the RAS signaling pathway, we used a RAS inhibitor to block these two MAPKs (fig. S5E). Because of the specific activation of p38 MAPK signaling in uSPG, we used a p38 inhibitor to explore its function in SSC. We validated the efficiency of inhibitors and activator used in this study by adding these chemicals with the median inhibitory concentration (table S7) to the cultured SSC for 4 days and then performed Western blotting analysis. The results showed that RAS inhibitors could effectively inhibit both Jnk and Erk MAPKs but not the p38 MAPK. The p38 MAPK inhibitor, PI3K-Akt inhibitor, YAP1 inhibitor (phosphorylation of YAP1), and YAP1 activator (dephosphorylation of YAP1) could all work effectively (fig. S5E). To exclude the indirect impact of these signaling pathways on SSC by regulating feeder cells [mitomycin C–treated mouse embryonic fibroblasts (MEFs)], MEFs were cultured in SSC culture medium and supplied with inhibitors/activators of specific signaling pathways for 4 days. SSC isolated from enhanced green fluorescent protein $(EGFP)^{Tg/+}$ mouse pups were enriched and cultured as previously described (*31*). $EGFP^+$ SSC were then inoculated into MEF and cultured for another 4 days without inhibitors/activators (fig. S5F). There was no significant variation in the number of SSC colonies under different conditions compared to that in the control group (fig. S5, G and H), suggesting that feeder cells treated with signaling pathway inhibitors or activators did not affect SSC culture, possibly because the feeder cells were in a nonproliferative state following mitomycin C treatment. Subsequently, $EGFP^+$ SSC were cultured with signaling pathway inhibitors/activators for 4 days (Fig. 3D). Colonies formed by cultured SSC and the expression of spermatogonial markers were detected. The colony size was significantly smaller in groups treated with p38, Ras, PI3K-Akt, or YAP1 inhibitors than in the control group (Fig. 3, E and F). Specifically, inhibition of p38, Ras, or YAP1 suppressed *Mki67* expression as well as expression of *Gfra1*, *Ret*, and *Zbtb16* that mark SSC or their uSPG progeny (Fig. 3G), suggesting impeded SSC maintenance and a reduced progeny population. Meanwhile, dSPG markers, including *Kit* and *Stra8*, were up-regulated, indicating enhanced SSC differentiation. In contrast, elevated expression of *Gfra1*, *Ret*, and *Zbtb16* and decreased expression of *Mki67* and *Kit* were observed upon inhibition of the PI3K-Akt signaling pathway, suggesting promoted SSC stemness (Fig. 3G).

Next, we performed transplantation assays to verify the role of these signaling pathways in SSC in vivo. After 4 days of culture, SSC treated with different inhibitors/activators were sorted via fluorescence-activated cell sorting (FACS) and transplanted into recipient mouse testes (Fig. 3D). Two months after transplantation, the number of colonies formed in the seminiferous tubules of recipient mice was evaluated. Inhibition of the PI3K-Akt signaling pathway enhanced colony formation after transplantation, whereas inhibition of the YAP1, p38, or Ras signaling pathway exerted the opposite effect, indicating their different roles in SSC maintenance (Fig. 3, H and I). Additional evidence was derived by inhibiting the Hippo pathway with a YAP1 activator (Fig. 3, E to I), confirming the unique role of the Hippo signaling pathway in promoting SSC differentiation and/or suppressing SSC stemness.

Identification of niche-derived paracrine factors regulating SSC maintenance

To identify key niche-derived paracrine factors related to the signaling pathways regulating SSC maintenance, we focused on the up-regulated paracrine factors per niche cell type under recovery conditions. Consistently, classical paracrine factors important for SSC maintenance, such as GDNF and FGF2 (*5*, *6*), were up-regulated in W, W3, and W5 mice (fig. S6A). In addition, compared to WT mice, FGF family members such as *Fgf18* (SER), *Fgf9* (MAC), *Fgf11* (SER), and *Fgf13* (SER) were up-regulated in W mice (fig. S6B). Nevertheless, *Fgf*5 was not detected in our data or in a previously reported single-cell dataset (GSE124263) probably because of its very low expression. To uncover potential secretory regulators as comprehensively as possible, both known and potentially secreted proteins that can exist in soluble form in the extracellular region or give rise to a secreted soluble extracellular domain (inferred from sequence or structural similarity from UniProt) were included. Differentially expressed paracrine factors were analyzed according to the respective niche cell type. For one specific niche cell type, differentially expressed genes (DEGs) were analyzed between samples using the Seurat function FindMarkers. Among the DEGs, paracrine factors that were up-regulated in W mice (W > WT) and further enhanced in W3 and W5 mice (W3 > W and W5 > W) for each niche cell type were identified (table S5).

We identified 20 paracrine factors that met the above conditions, six of which were highlighted in relation to signaling pathways regulating SSC maintenance (Fig. 4A and fig. S6C). These are *Igfbp7* (PI3K-Akt/ECM-receptor interaction), *Tek* (MAPK/PI3K-Akt), *Col4a2* (PI3K-Akt/ECM-receptor interaction), *Ccl24* (cytokine-cytokine receptor interaction), *Agt* (neuroactive L-R interaction), and *Tgfbr3* (TGF-β signaling pathway). On the basis of the UniProt

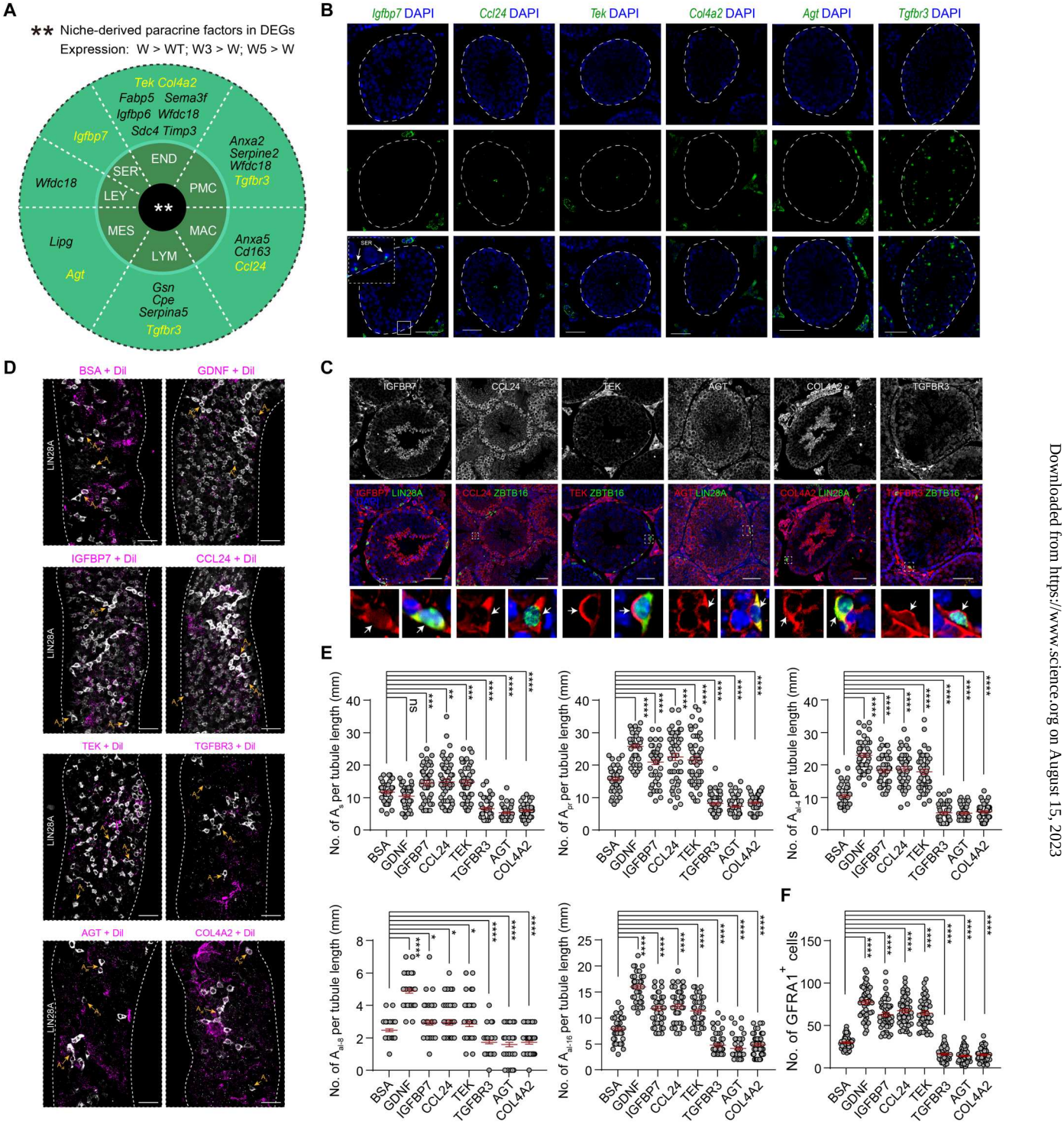

Fig. 4. Paracrine factors up-regulated under SSC recovery condition in mice. (**A**) Paracrine factors (W > WT; W3 > W; W5 > W) registered with individual niche cell types. (**B**) Fluorescence in situ hybridization for *Igfbp7*, *Ccl24*, *Tek*, *Col4a2*, *Agt*, and *Tgfbr3* (green) in the testis of adult mice. DAPI, 4′,6-diamidino-2-phenylindole. Scale bars, 50 μm. (**C**) Immunostaining of insulin-like growth factor binding protein 7 (IGFBP7), CCL24, TEK, TGFBR3, AGT, and COL4A2 (red) with LIN28A (green) or ZBTB16 (green) in the testis of adult mice. Scale bars, 50 μm. (**D**) Whole-mount images of a part of host seminiferous tubules showing LIN28A (white) and Dil (magenta) signals. Host seminiferous tubules were injected with microbeads pretreated with Dil and IGFBP7, TEK, CCL24, AGT, COL4A2, TGFBR3, GDNF (positive group), or bovine serum albumin (BSA; negative group), respectively. Scale bars, 50 μm. Densities of A_{single} (A_s), A_{paired} (A_{pr}), and $A_{aligned}$ (A_{al}), undifferentiated SPG (uSPG) (**E**), and GFRA1$^+$ uSPG (**F**). Each is presented by the number of corresponding cells contained in the 1-mm-long segment in Dil-positive areas after transplantation of soaked beads. Values represent means ± SEM (n = 50), and P values were obtained using one-way ANOVA followed by Tukey test. ($^{ns}P > 0.05$; $^{*}P < 0.05$; $^{**}P < 0.01$; $^{***}P < 0.001$; $^{****}P < 0.0001$).

Knowledgebase and previous studies, TEK receptor tyrosine kinase (TEK) (*32*) and transforming growth factor, beta receptor III (TGFBR3) (*33*), which are generally recognized as receptors, can produce secreted soluble extracellular domains; therefore, they were included as paracrine factors for further analysis. Single-cell transcriptome and fluorescence in situ hybridization revealed that these factors were expressed in different niche cells but were rarely expressed in SPG (Fig. 4B and fig. S6, D and E). We found almost no signal for *Ccl24*, *Tek*, *Col4a2*, or *Agt* in SPG located in the basement membrane of seminiferous tubules. The *Igfbp7* signal was detected in SER with typical vesicular nucleoli in the basement membrane but not in SPG, whereas the *Tgfbr3* signal was detected in SPG, SPC, SPT, and a subset of niche cells. Immunofluorescence assays showed that the protein signals of these factors were detected not only in niche cells but also in a subset of uSPG (Fig. 4C). These protein signals were present in the plasma membrane, cytoplasm, and/or nucleus of uSPG, marked by LIN28A or ZBTB16, suggesting the existence of active exchange, combination, and interaction of these paracrine factors between uSPG and their niche. In contrast, the protein signals of CCL24, angiotensinogen (AGT), collagen type IV alpha 2 (COL4A2), and TGFBR3 were also detected in dSPG ($ZBTB16^{-}$/$LIN28A^{-}$ in the basement membrane) and SPCs, indicating that these factors might play a role in regulating both spermatogonial differentiation and meiosis (Fig. 4C).

Functional validation of key paracrine factors for SSC maintenance

Six key paracrine factors were functionally validated in the context of SSC maintenance in vivo. We injected microbeads pretreated with different factors into the seminiferous tubules of WT mice to measure their function in regulating SSC activity (*34*), and GDNF (positive) and bovine serum albumin (BSA; negative) were used as controls. We analyzed the density of uSPG, including the A_{single} (A_s), A_{paired} (A_{pr}), and $A_{aligned}$ (A_{al}) subpopulations, to evaluate changes in the stemness or differentiation properties of SSC. Five days after injection, the density of uSPG surrounding the microbeads was measured via whole-mount immunofluorescence (Fig. 4D). The results showed that IGFBP7, TEK, and CCL24 enhanced the density of A_s, A_{pr}, $A_{al\text{-}4}$, $A_{al\text{-}8}$, and $A_{al\text{-}16}$ cells and number of glial cell line derived neurotrophic factor family receptor alpha 1 positive ($GFRA1^{+}$) SPG, as opposed to AGT, COL4A2, and TGFBR3 (Fig. 4, E and F, and fig. S5I), indicating the specific role of IGFBP7, TEK, and CCL24 in promoting SSC stemness and proliferation.

These findings were validated using SSC cultured in vitro. The indirect impact on SSC through feeder cells was ruled out, as the SSC colony formed on feeder cells treated with different factors was comparable to that of the control group (fig. S7, A and B). The cultured SSC were then treated with individual factors for 4 days. Colonies formed by cultured SSC and the expression of spermatogonial markers were examined, and SSCs were synchronously transplanted into recipient mouse testes (Fig. 5A). We examined the effect of TEK on MAPK and PI3K-Akt signaling pathways and the effect of COL4A2 on PI3K-Akt signaling pathway in in vitro–cultured SSC. Four days after treatment, ERK1/2 and SAPK/JNK were activated, and Akt was inhibited in SSC supplied with TEK, while Akt was activated in SSC supplied with COL4A2 (fig. S7C). These results indicated that TEK and COL4A2 may function partially via activation of related signaling pathways. We found that IGFBP7, CCL24, and TEK promoted SSC colony formation; up-regulated the expression of *Mki67*, *Zbtb16*, *Gfra1*, and *Ret*; and enhanced in vivo SSC survival after transplantation (Fig. 5, B to E), confirming their roles in supporting SSC proliferation and stemness. Opposite results were observed for AGT, COL4A2, and TGFBR3, which were characterized by smaller and fewer SSC colonies; lower expression of *Zbtb16*, *Gfra1*, and *Ret*; and lower SSC survival after transplantation (Fig. 5, B to E), suggesting their roles in suppressing SSC stemness. In addition, AGT and TGFBR3 enhanced the expression of *Kit* and *Mki67*, indicating their role in promoting SSC proliferation and differentiation (Fig. 5D).

Next, we generated $Ccl24^{-/-}$, $Igfbp7^{-/-}$, and $Agt^{-/-}$ mice to validate the function of IGFBP7, CCL24, and AGT in SSC maintenance in vivo ($Tek^{-/-}$, $Col4a2^{-/-}$, and $Tgfbr3^{-/-}$ mice were embryonically lethal). Immunofluorescence staining showed complete knockout (KO) of IGFBP7, CCL24, and AGT in the respective KO mice (fig. S7D). We found no significant difference in the number of SPG between postnatal (PND1 and PND7) WT and KO mice (fig. S7E). In adult mice, the serum hormone levels of testosterone, follicle-stimulating hormone (FSH), and luteinizing hormone (LH) did not significantly change in KO mice (fig. S7F). Although both adult $Ccl24^{-/-}$ and $Igfbp7^{-/-}$ mice exhibited normal body weights, we found progressive degeneration in male reproduction and gradual loss of the SSC pool, characterized by smaller testes, reduced sperm count in the epididymis, increased degenerated seminiferous tubules, and reduced number of $GFRA1^{+}$ SPG (Fig. 6, A to D; and figs. S7G and S8, A to C). Sertoli-only seminiferous tubules in $Ccl24^{-/-}$ and $Igfbp7^{-/-}$ mice showed diminished expression of *Mki67* and uSPG markers (Fig. 6E and fig. S8D). The number of $LIN28A^{+}$ uSPG and ratio of $MKI67^{+}LIN28A^{+}$/$LIN28A^{+}$ uSPG were significantly decreased in $Ccl24^{-/-}$ and $Igfbp7^{-/-}$ mice (Fig. 6E). Consequently, the SSC pool decreased, accompanied by gradual germ cell loss and vacuolization of seminiferous tubules. In contrast, slightly smaller testes and a small fraction of vacuolar seminiferous tubules were found in adult $Agt^{-/-}$ mice without significant differences in either the haploid number of epididymis or expression of uSPG and dSPG markers (Fig. 6, A to D; and figs. S7G and S8, A to D), suggesting that AGT is dispensable for spermatogonial differentiation. However, despite the insignificant impact of *Agt* KO on the total number of $GFRA1^{+}$ SPG and $LIN28A^{+}$ uSPG and ratio of $MKI67^{+}LIN28A^{+}$/$LIN28A^{+}$ uSPG, AGT appeared to contribute to long-term SSC maintenance, as germ cells in vacuolar seminiferous tubules were partially depleted in $Agt^{-/-}$ mice (Fig. 6E). Furthermore, we transplanted WT SSC into 2-month-old WT, $Ccl24^{-/-}$, $Igfbp7^{-/-}$, and $Agt^{-/-}$ mice, which were used as recipient mice after 1 month of treatment with busulfan (40 mg/kg). Two months after transplantation, the testes of recipient mice were harvested and observed under a fluorescence microscope. The number of colonies formed after transplantation significantly reduced in $Ccl24^{-/-}$ and $Igfbp7^{-/-}$ mice, whereas no significant difference was observed between WT and $Agt^{-/-}$ mice (fig. S8E).

Dysregulated niche-derived paracrine factors associated with human infertility

To evaluate the relevance of newly identified factors in human spermatogenesis, we analyzed their expression in normal human testes using the human scRNA-seq dataset (GSE124263) (*12*). Most of these niche-derived paracrine factors showed low transcriptional expression in human SSC (Fig. 7A), which was consistent with

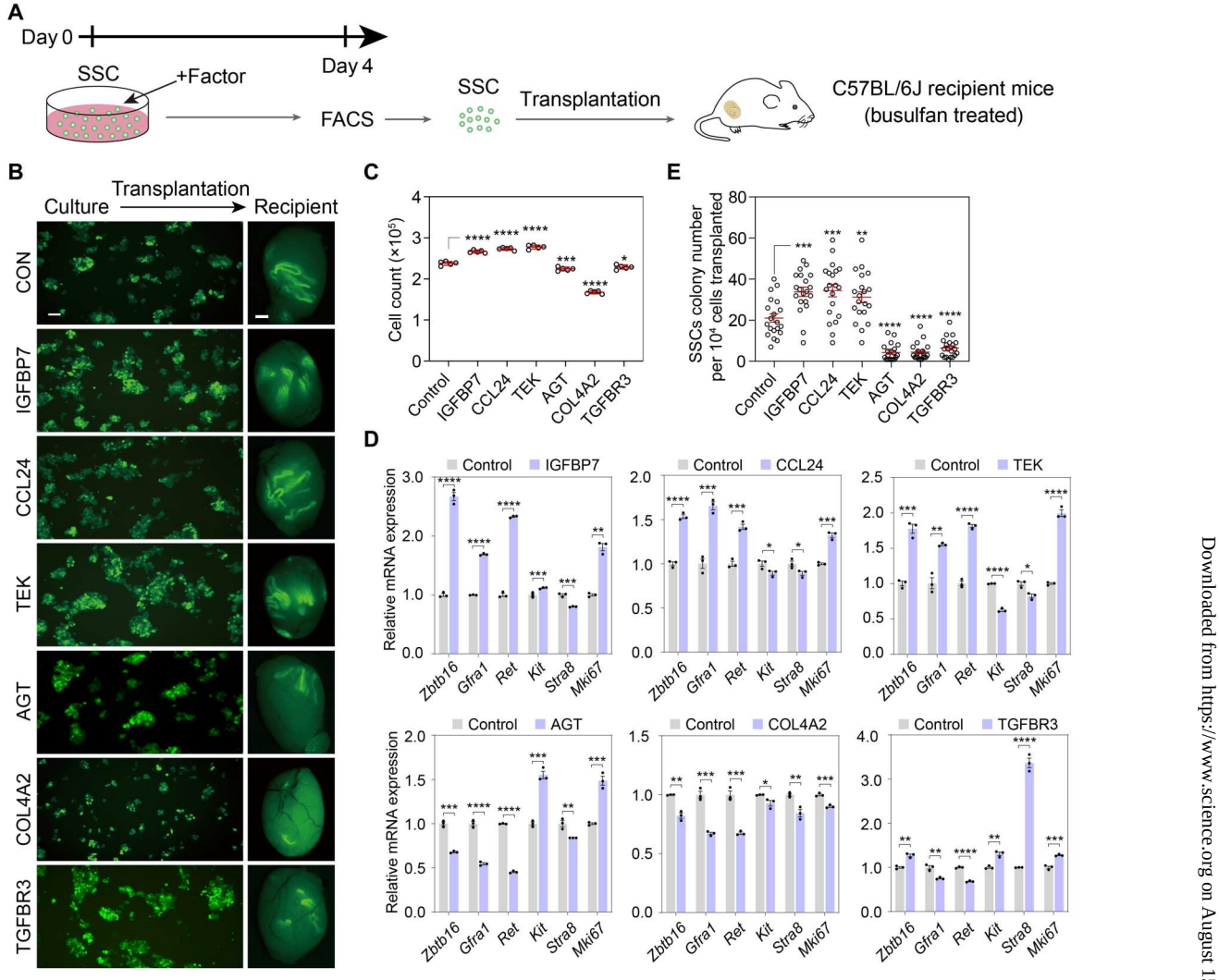

Fig. 5. Functional validation of the up-regulated paracrine factors via in vitro SSC culture and transplantation assays. (**A**) Strategy for functional validation of candidate paracrine factors specified (W > WT; W3 > W; W5 > W) in the cultured SSC. (**B**) In vitro SSC culture and transplantation assay. Individual image (culture) represents donor SSC after 4 days of culture with the corresponding factor (scale bar, 50 μm). The recipient testes were examined 2-months after the transplantation (scale bar, 1 mm). (**C**) Cell number of in vitro–cultured EGFP$^+$ SSC 4 days after coculture with corresponding factor (n = 5). Values represent means ± SEM, and P values were obtained using one-way ANOVA followed by Tukey test (*P < 0.05; ***P < 0.001; ****P < 0.0001). (**D**) Quantitative RT-PCR analysis of SPG markers in the cultures supplied with different factors. Values represent means ± SEM (n = 3), and P values were obtained using two-tailed t tests (*P < 0.05; **P < 0.01; ***P < 0.001; ****P < 0.0001). (**E**) The numbers of SSC colonies formed in the recipient testes per group (n = 20). Values represent means ± SEM, and P values were obtained using one-way ANOVA followed by Tukey test (**P < 0.01; ***P < 0.001; ****P < 0.0001).

the results in mice. Further immunostaining revealed high IGFBP7 signals in GATA4$^+$ SER and SPG in the basement membrane of seminiferous tubules, whereas CCL24, AGT, TEK, and TGFBR3 showed relatively low signals in SPG (Fig. 7B). COL4A2 signals were detected in GATA4$^+$ SER, SPG in the basement membrane, and interstitial niche cells (Fig. 7B). The expression of these factors in the human testes was similar to that in murine testes, indicating their potentially similar functions in humans.

The expression relevance of newly identified factors in infertile patients was analyzed by referring to the GSE108886, GSE145467, and GSE45885 datasets, and 13 factors showed elevated expression in these patients (Fig. 7C and table S6). In parallel, we examined the potential genetic variations/alternations of newly identified factors in 314 Chinese patients with azoospermia using the whole-exome sequencing dataset (GSE112013). Deleterious single-nucleotide polymorphism (SNP) mutations (missense variant SNP, sort intolerated from tolerated (SIFT)_score < 0.05) were identified in the 13 factors (Fig. 7D and table S6). Notably, *COL4A2*, *CPE*, and *GSN* showed high SNP mutation frequencies in infertile patients (Fig. 7D), and SNP mutations (rs141883791 in *TGFBR3*, rs201647127 in *COL4A2*, and rs375261929 in *AGT*) were recorded in an independent SNP database (www.ncbi.nlm.nih.gov/SNP).

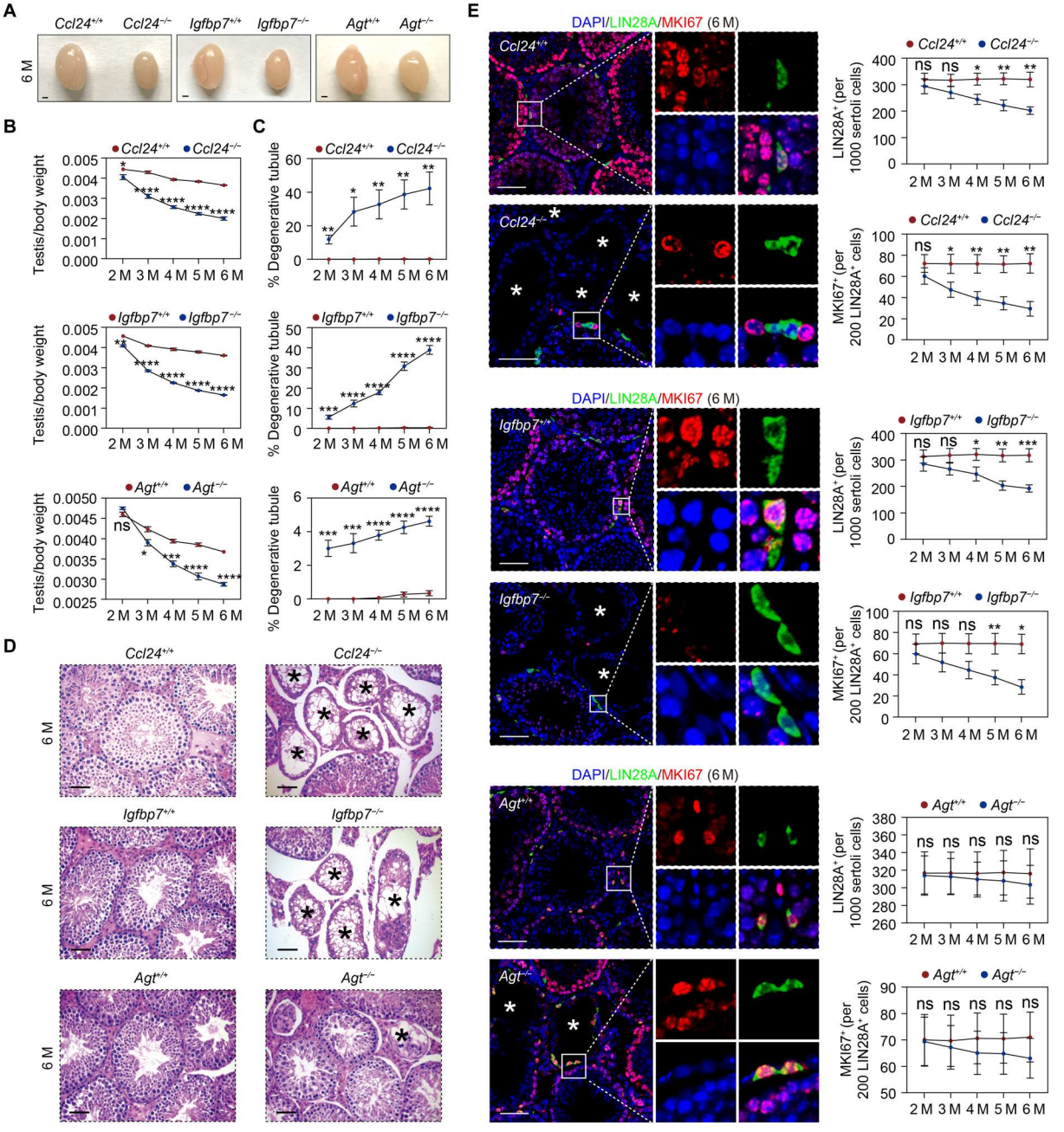

Fig. 6. Progressive SSC loss and oligozoospermia phenotype in *Ccl24*$^{-/-}$, *Igfbp7*$^{-/-}$, and *Agt*$^{-/-}$ mice. Testes size (**A**), testis weight/body weight (**B**), and degenerative seminiferous tubules (**C**) of *Ccl24*$^{-/-}$, *Igfbp7*$^{-/-}$, and *Agt*$^{-/-}$ mice, respectively ($n = 5$). M, month. Values represent means ± SEM, and P values were obtained using two-tailed t tests ($^{ns}P > 0.05$; $^{*}P < 0.05$; $^{**}P < 0.01$; $^{***}P < 0.001$; $^{****}P < 0.0001$). (**D**) Representative hematoxylin and eosin staining pictures of the testes from respective knockout (KO) mice (6 months old, $n = 5$). The degenerative tubules are highlighted with asterisks. (**E**) The expressions of LIN28A (green) and antigen identified by monoclonal antibody Ki 67 (MKI67) (red) and corresponding cell densities in the seminiferous tubules of 6-month-old KO mice ($n = 10$). The degenerative tubules are highlighted with asterisks. Values represent means ± SEM, and P values were obtained using two-tailed t tests ($^{ns}P > 0.05$; $^{*}P < 0.05$; $^{**}P < 0.01$; $^{***}P < 0.001$). Scale bars, 1 mm [in (A)] and 50 μm [in (D) and (H)].

DISCUSSION

With recent advances in single-cell transcriptome profiling, many studies have provided insights into SSC behavior and regulation, highlighting the heterogeneity of SSC and focusing on characterizing the nature of SSC. Within the uSPG population, many genes such as *Gfra1*, *ID4*, *Ret*, *Etv5*, *Eomes*, *Pax7*, *Nanos2*, *Shisa6*, *T*, *Pdx1*, *Lhx1*, *Egr2*, *Plvap*, *FGFR3*, *UTF1*, *PIWIL4*, and *TSPAN33* with relatively high expression in primitive subfractions have been identified and investigated (*35*–*45*). Particularly, *Gfra1*, *ID4*, *Eomes*, *Pax7*, *Nanos2*, and *Plvap* have been further validated as SSC markers through lineage tracing experiments, which are reliable methods for studying the origin and development of stem cells.

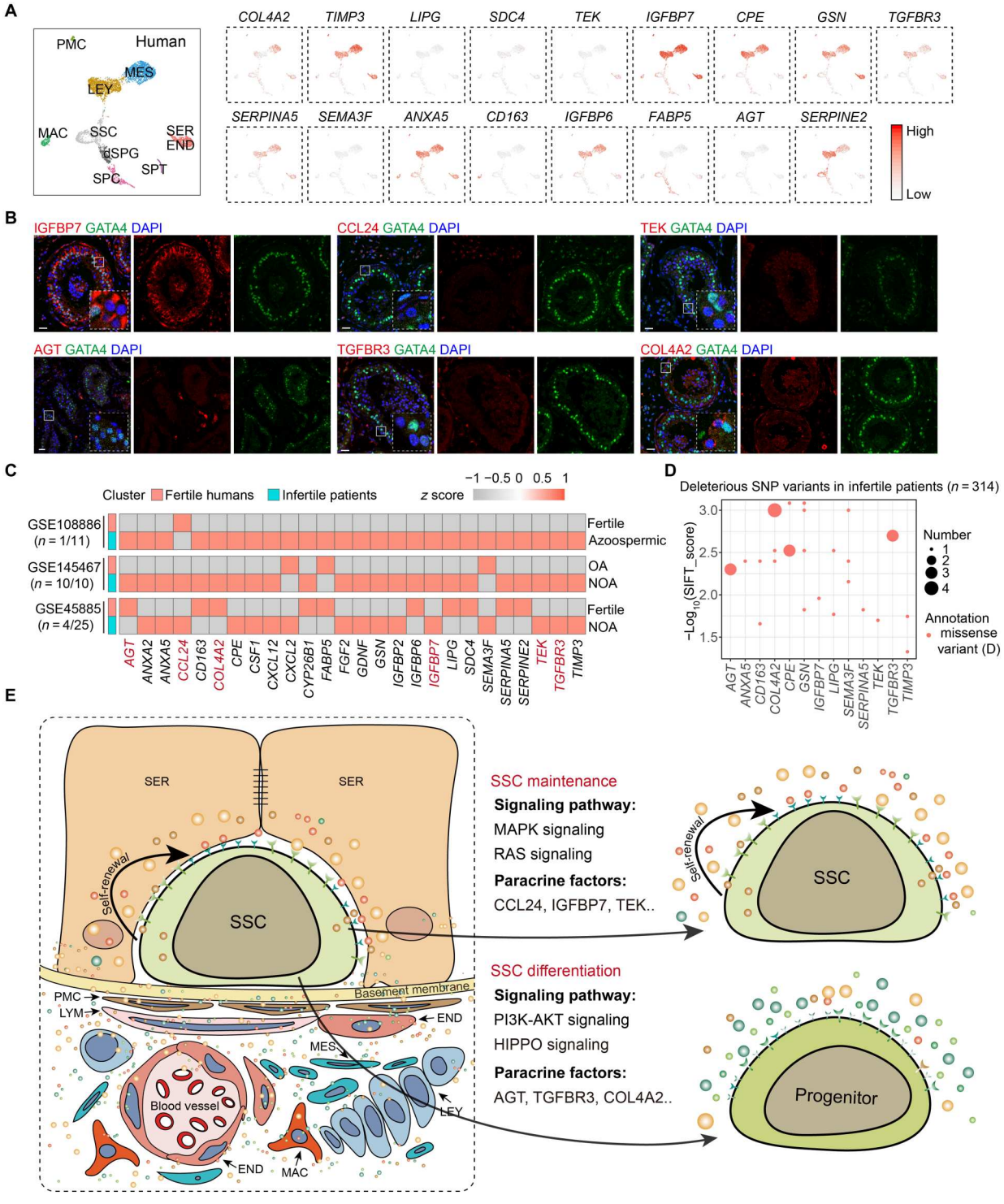

Fig. 7. The clinical relevance of the newly found paracrine factors to human infertility. (**A**) Feature plots for the human homologous genes of the newly found paracrine factors as referring to the single-cell RNA sequencing (scRNA-seq) dataset (GSE124263). (**B**) Immunostaining for GATA4 (green) and corresponding factors (red) in human testes. Scale bars, 25 μm. (**C**) Heatmap based on the expression of corresponding factors in patients with impaired spermatogenesis and azoospermia (GSE108885, GSE145467, and GSE45885) (*n* = fertile human number/infertile patients number). (**D**) Deleterious SNP mutations frequencies in the genes encoding corresponding factors in the genomes of 314 infertile patients (GSE112013). (**E**) Model of the key signaling pathways and paracrine factors regulating SSC maintenance (self-renewal) or differentiation validated in this study.

In this study, for characterizing the cluster enriched for SSC from the SPG population, we used classic stem cell markers such as *Gfra1*, *Ret*, *Etv5*, and *Eomes* in mice as well as *FGFR3*, *UTF1*, *ID4*, *PIWIL4*, and *TSPAN33* in humans.

SSC maintenance and differentiation are regulated by the testicular niche. To the best of our knowledge, this is the first comprehensive atlas of SSC regulation characterized by niche-dependent interactions, including L-R pairs and cell-cell connections, and signaling pathways transduced by paracrine factors in adult mice and humans under physiological conditions. Compared to the limited somatic cell–specific L-R pairs that regulate SSC, most L-R pairs showed great overlap among different niche cells in both mice and humans. The widespread expression of paracrine factors in multiple niche cell types ensures the stable supplementation of paracrine factors for regulation of SSC, which can protect against the impact of loss of expression of these factors in one specific niche cell type. Further functional validation is required to specifically inactivate the receptors of these paracrine factors in SSC either genetically or chemically. Moreover, in addition to the currently known L-R pairs that have been confirmed using biological experiments, the receptors of most paracrine factors in the testes are unknown and need to be further explored. Therefore, our study provides a resource for further exploration of the intercellular paracrine regulation of testicular niche cells during SSC fate commitment in mice and humans.

The "recovery" model using WT mice with busulfan treatment is an ideal model that could provide useful and more applicable insights for sperm cell regeneration. However, except for a 95% loss of SPG, the majority of germ cells at different stages remained in WT mice for at least 3 weeks after busulfan injection (*1*, *46*). Therefore, to detect the response of niche cells to the progressive or rapid loss of SSC without interference from feedback regulation between niche and germ cells at different stages of differentiation, we selected W mice as an impaired model with induced SSC recovery effect. Note that compared with WT mice, the SSCs and somatic cells in W mice may be developmentally abnormal due to the *Kit* mutation. To circumvent defects in the application of W mice that may confound the analysis, we used the following strategy to guarantee that cell-cell interactions existed under physiological conditions: First, we analyzed interactions between SSC and niche cell using the WT mouse model, and then the interactions existing in both WT and W mice models were selected as potential regulators for SSC maintenance. In addition, although we cannot exclude the signals for promoting SSC differentiation in W mice, this model helps us highlight signals that can promote SSC maintenance, in which the more dominant trend in stem cell maintenance under regenerative conditions could allow us to focus more on the potential factors regulating SSC maintenance.

The notion that the SER and interstitial somatic cells play essential roles in regulating SSC was reflected and elaborated to a greater extent in this study. We found intense and hyperactive connections between LEY, MES, END, SER, and SSC in mice and humans. Our data highlighted the contribution of END and MAC to SSC maintenance, characterized by a great number of interactions and signaling pathways transduced between END/MAC and SSC. This was further supported by reports describing the preferential localization of SSC in the tubular regions adjacent to the vasculature, where END and MAC cells localize and produce paracrine factors to support SSC self-renewal (*34*, *47*, *48*). As highlighted in this study, TEK is a paracrine factor derived from END that is essential for maintaining SSC stemness. We also demonstrated that CCL24 mediated the role of MAC in regulating SSC maintenance, complementing a previously reported role of CCL24 in regulating SSC differentiation (*48*).

In this study, we highlighted the essential roles of CCL24, IGFBP7, and TEK in SSC maintenance and confirmed the differentiation-promoting functions of HIPPO signaling pathway, AGT, TGFBR3, and COL4A2 in SSC fate commitment (Fig. 7E). Recently, YAP1 has been reported to be nonessential for spermatogenesis (*49*). However, inactivation of Hippo signaling is vital for stem cell self-renewal and tissue regeneration (*9*, *50*). Our study found that inhibition of YAP1 impaired SSC maintenance, highlighting the need to further investigate the role of Hippo signaling in long-term SSC maintenance. Although its potential roles in stem cell maintenance have been proposed in other tissues, our work provides the first experimental evidence of the essential roles of CCL24 and IGFBP7 in SSC maintenance. IGFBP7, as an inhibitor of insulin/IGF signaling, affects the differentiation of both stem cells and SPG by interfering the activation and internalization of IGF1 receptor (IGF1R) and blocking its downstream PI3K signaling pathway (*51*, *52*). Our work prompted IGFBP7′s role in maintaining SSC stemness by competing with IGF1 for binding to IGF1R, thereby suppressing the downstream PI3K signaling pathway. We also identified AGT, COL4A2, and TGFBR3 as specific factors involved in SSC differentiation, consistent with previous findings on other tissue formation processes (*53*, *54*). Meanwhile, newly identified factors such as annexin A2 (ANXA2) and serine (or cysteine) peptidase inhibitor, clade E, member 2 (SERPINE2), which function in cell differentiation in other tissues (*55*), may also be required for SSC differentiation, although further studies are needed.

The majority of newly identified factors showed deleterious SNP mutations and/or up-regulation in infertile patients with azoospermia or non-obstructive azoospermia (NOA), which reflected similar responses of testicular niche cells to depletion of germ cells in the human testes. Because we did not have a detailed pathology or case information on these infertile patients, we could not perform further analysis. Therefore, the analysis results here only reflect the potential relevance of the up-regulation/loss of function of these factors in human infertility. Defects in infertile patients may occur at different stages of spermatogenesis, and the ideal data for analyzing the relevance of these factors to human SSC maintenance would be from human patients who before being diagnosed with infertility symptoms undergo biopsies in the hospital to show gradual exhaustion of the SSC pool. Although it is difficult to meet such patients, we will continue to find them in the future to analyze our data.

In summary, this study revealed the conservation of paracrine factors and related signaling pathways between mice and humans under both physiological and pathological conditions. Key paracrine factors identified in SSC regeneration were also associated with human infertility. We also found that essential paracrine factors, such as IGFBP7, TEK, and CCL24, enhance the survival, proliferation, and development of murine donor SSC after transplantation, which may lead to future human therapeutic opportunities. This work also provides a framework for discovering and validating the factors essential for SSC maintenance, which can not only help overcome the outstanding challenge in the long-term culture of human SSC but also serve as a reference for

future studies on the aetiology, diagnosis, and treatment of male infertility.

MATERIALS AND METHODS

Mice

All animal experiments were approved by the Committee on Animal Care of Institute of Basic Medical Sciences Chinese Academy of Medical Sciences, School of Basic Medicine, Peking Union Medical College. Eight-week-old C57BL/6J WT mice and W mice were used. W mice were obtained by crossing the Kit^{W} mice (the Jackson Laboratory, stock no. 000692) with Kit^{Wv} mice (the Jackson Laboratory, stock no. 000692). Busulfan (15 mg/kg) was intraperitoneally injected into W mice, and the testes were harvested after 3 or 5 days (W3 and W5). $Igfbp7^{+/-}$ (Cyagen Biosciences, stock no. KOCMP-29817-Igfbp7), $Ccl24^{+/-}$ (Cyagen Biosciences, stock no. KOCMP-02289-Ccl24), and $Agt^{+/-}$ (Cyagen Biosciences, stock no. KOCMP-11606-Agt) mice were bred for homozygous KO mice. Eight-week-old C57BL/6J WT mice were treated with busulfan (40 mg/kg) and used as recipients for the transplantation assay 1 month later. $EGFP^{Tg/+}$ mice (the Jackson Laboratory, stock no. 021930) were used as donors of cultured SSC. All mice were housed and bred under specific pathogen–free conditions (temperature: 22° to 26°C, humidity: 40 to 55%, 12-hour light/dark cycle) in the animal facility of Institute of Basic Medical Sciences. DNA was isolated from the tail, and the genotypes of mice were checked using polymerase chain reaction (PCR). The primer sequences are listed in table S7. All mice were randomly assigned to the experiments, and no statistical methods were used to predetermine the sample size. The person performing the experiments did not know the sample identity until after data analysis. No data were excluded from the analyses, and the displayed data included a minimum of three independent experiments with a minimum of three biological replicates for each independent experiment.

Single-cell RNA-seq

Testes from WT, W, W3, and W5 mice were minced and digested with collagenase type IV (1 mg/ml; Sigma-Aldrich) and deoxyribonuclease I (DNase I; 500 μg/ml; Sigma-Aldrich) at 37°C for 15 min. The cell suspension was pipetted up and down once every 5 min, and the digestion process was stopped using Dulbecco's modified Eagle's medium containing 10% fetal bovine serum (FBS). Under each condition, testicular single-cell suspensions from three biological replicates were mixed and filtered through a 40-μm nylon mesh. After centrifugation, the cells were resuspended in 0.04% BSA in phosphate-buffered saline (PBS) for loading onto the Chromium Single Cell 3′ Chip kit v2 (10x Genomics, PN-120236). Cell capture and library preparation were performed following the instructions of Chromium Single Cell 3′ v2 Library and Gel Bead Kit (10x Genomics, PN-120237). Briefly, 10,000 cells were targeted for capture per sample, and after cDNA synthesis, 10 to 12 cycles were used for library amplification. The libraries were then size-selected, pooled, and sequenced on a NovaSeq 6000 (Illumina). Shallow sequencing was performed to assess library quality and adjust the subsequent sequencing depth based on the capture rate and detected unique molecular indices (UMIs).

scRNA-seq data processing

Raw sequencing reads were processed using Cell Ranger v.3.0.1 on the 10x Genomics platform. Briefly, reads from each sample were demultiplexed and aligned to the mouse mm10 genome, and UMI counts were quantified for each gene per cell to generate a gene barcode matrix. The matrix from each sample (WT, W, W3, and W5) was aggregated and normalized to the same sequencing depth, resulting in a combined gene-barcode matrix for all samples. Default parameters were used, and the UMI counts of different samples were analyzed using the Seurat R Package (v.3.0.1) (*56*) following the Seurat pipeline. Cells with more than 200 detected genes or fewer than 20% mitochondrial reads (10% in WT) were retained. Genes not detected in at least three cells were removed from subsequent analyses. The resulting matrix was normalized, the most variable genes were identified using Seurat's default settings, and the matrix was scaled with regression against mitochondrial reads. The top 2000 variable genes were used to perform principal components analysis, and jackstraw analysis was performed using Seurat's default settings. Variations in cells were visualized using UMAP for the top principal components. To identify marker genes for each cell type, the Seurat function FindAllMarkers with default settings was used to identify up-regulated genes in each cluster compared to other cells. Cell types were determined using the marker genes identified in literature. The SPG cluster was reclustered using the same method that was used to characterize the SSC population. We used the Seurat function CellCycleScoring to determine the cell cycle phase, because this program determines the relative expression of a large set of G_2-M and S phase genes. The Seurat function FeaturePlot and VlnPlot were used to plot specific genes.

For integrated analysis of W, W3, W5, and WT, the combined gene-barcode matrix of all samples was analyzed following Seurat's default pipelines. Cells with more than 200 detected genes or fewer than 20% of mitochondrial reads were retained. Genes not detected in at least three cells were removed from subsequent analyses. The joint dataset was scaled and visualized using t-distributed stochastic neighbor embedding (t-SNE) for the top 30 principal components. Testicular cell types were characterized according to marker expression. After removing SPC, SPT, and undefined cells, the remaining niche cells and SPG were reclustered using the same method. The Seurat function FindMarkers with default settings was used to identify genes that were up-regulated in a specific cluster compared to another. Differentially expressed paracrine factors were analyzed according to the respective niche cell type. For a specific niche cell type, the DEGs were analyzed between samples using the Seurat function FindMarkers. Paracrine factors of each niche cell type that were up-regulated in W mice (W > WT) and further increased in W3 and W5 mice (W3 > W and W5 > W) were identified.

The overall SPG in WT, W, W3, and W5 was used for trajectory analysis, and a single-cell pseudotime trajectory was constructed using the Monocle 2 package (v2.12.0) (*57*) according to the provided documentation. The Monocle functions clusterCells and differentialGeneTest were used to detect cell clusters and DEGs between clusters (q value < 0.01). The top 1000 DEGs were used for ordering cells, and the discriminative dimensionality reduction with the trees (DDRTree) method was used to reduce the data to two dimensions. Dynamic expression patterns with the spermatogonial

developmental trajectory of specific genes were visualized using Monocle function plot_genes_in_pseudotime.

Human dataset analysis

Processing data of the adult single-cell human testes dataset were downloaded from the Gene Expression Omnibus (GEO) GSE124263, and the UMI counts were analysed using Seurat R Package (v.3.0.1) following the Seurat pipeline with the same parameters and functions as previously mentioned. On the basis of classic markers, we characterized the niche cell types and uSPG. SER and END in the human dataset were clustered in the same cluster. The relative expression of up-regulated paracrine factors in patients with impaired spermatogenesis or NOA phenotypes (according to the datasets GSE108886, GSE145467, and GSE45885) compared to the respective control groups was analyzed using GEO2R.

L-R interaction analysis

The subcellular localisation of genes was characterized using the UniProt Knowledgebase (www.uniprot.org). To cover potential secretory regulators as comprehensively as possible, both known secreted proteins and potential secretory proteins, which can exist in soluble form in the extracellular region or give rise to a secreted soluble extracellular domain (inferred from sequence or structural similarity from UniProt), were included. On the basis of the established L-R interactions from the CellPhoneDB and FANTOM5 databases, with the incorporation of immune-relevant cytokines, chemokines, coinhibitors, costimulators, and their receptors, the ligands and receptors expressed in each cell type of each sample were obtained, and the L-R pair expressed in niche cells (ligand) and SSC (receptor) was selected to build intercellular interactions. The respective L-R pairs between each niche cell type and SSC in each sample were used to build potential interactions using Cytoscape (v3.8.1). The L-R pairs between niche cells and SSC in the human dataset were characterized using the same method, and the L-R pairs shared between humans and mice were characterized.

Enrichment analyses

GO and KEGG pathway enrichment analyses were conducted using the ClusterProfiler package (v3.12.0) and ClueGO app (v2.5.7) in Cytoscape (v3.8.1) with default settings and a cutoff *P* value of 0.05. GSEA was performed using the GSEA (v4.0.2) algorithm with MSigDB (v7.0) using default settings. Signaling pathways enriched in niche-derived paracrine factors and uSPG-derived membrane proteins in DEGs of the four samples were characterized. For each niche cell type, the niche-derived signaling pathways in all four samples overlapped with the SSC-derived signaling pathways to identify candidate signaling pathways pivotal to SSC maintenance.

Culture and transplantation assay of SSC

SSC were isolated, enriched, and cultured as previously described (*31*). Briefly, a testicular cell suspension of PND5 to PND6 $EGFP^{Tg/+}$ mice pups was obtained using a two-step enzymatic digestion protocol with type IV collagenase (1 mg/ml; Sigma-Aldrich), trypsin (0.25%; Invitrogen), and DNase I (500 μg/ml; Sigma-Aldrich). The dissociated cells were centrifuged, resuspended in Dulbecco's PBS containing 1% FBS (Gibco), and centrifuged in 30% Percoll solution. SPG were enriched using MACS to isolate $Thy1^+$ cells. The $EGFP^+$ SSC were cultured on the MEF treated with mitomycin C (Sigma-Aldrich) in serum-free minimum essential medium α (MEMα; Gibco) supplemented with other components as previously described.

In this study, SSC supplemented with GDNF (10 ng/ml; R&D Systems) were cultured with specific factors, inhibitors, or activators of signaling pathways following the manufacturer's instructions (concentrations are listed in table S7). For SSC cultured with signaling inhibitors/activators, transplantation assays of $EGFP^+$ SSC sorted using FACS were performed at 48 hours. Colony formation and cell number of SSC were analyzed after 4 days of culture followed by gene expression analysis. The colony sizes (volumes) of SSC observed under a fluorescence microscope reflected the self-renewal and/or proliferation properties of cultured SSC. For SSC cultured with paracrine factors, the colony size, cell number, and gene expression of SSC were analyzed after 4 days of culture followed by transplantation assays of $EGFP^+$ SSC sorted using FACS.

For the transplantation experiment, 8-week-old C57BL/6J WT mice were treated with busulfan (40 mg/kg) and used as recipient mice 1 month later. The same number of cells was transplanted into different groups (1×10^4 cells per recipient testis). Two months after transplantation, recipient mouse testes were harvested and observed under a fluorescence microscope. A network or patch was defined as a colony that occupied more than 50% of the basal surface of tubule and was at least 0.1 mm in length (*58*). The number of colonies counted in the seminiferous tubules of recipient mice represents the number of functional SSC.

For the control experiment, MEFs treated with mitomycin C were cultured in serum-free MEMα (Gibco) supplemented with other components as previously described (*31*) and treated with specific factors or inhibitors/activators of signaling pathways for 4 days. SSC were then inoculated into MEF and cultured for another 4 days without factors or inhibitors/activators.

Microbead preparation and transplantation

Affi-Gel blue beads (Bio-Rad) were soaked in a solution of recombinant GDNF, IGFBP7, TEK, CCL24, TGFBR3, AGT, and COL4A2 proteins (0.1 mg/ml) or 0.1% BSA at room temperature for 1 hour, as previously described (*34*). To mark the tubular wall adjacent to the transplanted beads, the beads were immersed in DiI solution (0.83 mg/ml; Thermo Fisher Scientific) for 15 min. For the transplantation assay, soaked beads were transplanted into the testicular interstitium [one or two beads (one per site) separated at appropriate intervals] via a vitrified microcapillary under a dissecting microscope.

Immunofluorescence

Paraffin-embedded human testis tissue fixed with 4% (v/v) paraformaldehyde was obtained from Peking University First Hospital. The experiments performed in this study were approved by the Ethics Committee of Institute of Basic Medical Sciences Chinese Academy of Medical Sciences, School of Basic Medicine, Peking Union Medical College. Mouse testes were fixed in 4% paraformaldehyde (PFA) at 4°C overnight, dehydrated, and embedded in paraffin and cut into 5-μm-thick sections. The rehydrated sections were subjected to antigen retrieval, blocked in 5% BSA with 0.1% Triton X-100, and incubated with the primary antibody (table S7) at 4°C overnight. After three 5-min washes in PBS, the sections were incubated with secondary antibodies (table S7) and DAPI (4′,6-diamidino-2-phenylindole; Sigma-Aldrich) at 37°C for 1 hour. After

three 5-min washes in PBS, the coverslips were mounted on glass slides using anti-quencher fluorescence decay (Solarbio). Images were captured using a Zeiss 780 laser scanning confocal microscope.

Whole-mount immunofluorescence

Whole-mount immunofluorescence of seminiferous tubules was performed as previously described (*59*). Briefly, seminiferous tubules were disentangled from testicular biopsies and immediately fixed in 4% PFA at 4°C for 4 hours. After fixation, the seminiferous tubules were permeabilized with 0.5% Triton X-100 in PBS and treated with 1% BSA and 5% normal donkey serum in PBS at 4°C overnight. After three 30-min washes, the seminiferous tubules were incubated with primary antibody (table S7) at 4°C overnight. After three 30-min washes, the seminiferous tubules were washed three times for 30 min each and incubated with species-specific secondary antibodies and DAPI at room temperature for 2 hours. After three 30-min washes, the seminiferous tubules were mounted on slides with anti-quencher fluorescence decay (Solarbio) and observed using a Zeiss 780 laser scanning confocal microscope. LIN28A is predominantly expressed in the cytoplasm with punctate nuclear staining in all uSPG and can mark the length of cell chains (*60*). To analyze the whole-mount staining of seminiferous tubules, we classified the number of chained cells according to a previous study (*60*, *61*). A_{pr} and A_{al} SPG were interconnected by intercellular cytoplasmic bridges due to incomplete cytokinesis, and the frequencies of LIN28A$^+$ A_s, A_{pr}, and A_{al} SPG were identified on the basis of authentic morphological criteria. We counted seminiferous tubules of sufficient length that are long enough to average the entire seminiferous epithelial cycle.

RNA isolation and quantitative RT-PCR analysis

Total RNA was extracted from the testes or cultured cells using the RNeasy Kit (QIAGEN), reverse-transcribed using the RevertAid First Strand cDNA Synthesis kit (Thermo Fisher Scientific), and processed for quantitative reverse transcription polymerase chain reaction (RT-PCR) using the PowerUp™ SYBR™ Green Master Mix (Applied Biosystems) and LightCycler 480 system (Roche) with gene-specific primers (table S7). The reactions were run in triplicate, and mRNA levels were normalized to *Gapdh* and quantified using the delta-delta C_t method. The values shown are means ± SEM from three biological replicates. Primer sequences for each gene are listed in table S7.

Western blotting

The lysates of SSC were prepared in radioimmunoprecipitation assay lysis buffer (Biomed, Shanghai) supplemented with protease inhibitor cocktail tablets (Roche) and 1 mM phenylmethylsulfonyl fluoride. The homogenate was centrifuged at 16,000*g* for 10 min at 4°C, and the supernatants were used for subsequent analyses. After electrophoresis on 10% SDS–polyacrylamide gel electrophoresis gels, proteins were transferred to polyvinylidene difluoride membranes and blocked in 5% skimmed milk. The membranes were incubated with primary antibody (table S7) at 4°C overnight and horseradish peroxidase–labeled secondary antibody (table S7) for 1 hour at 37°C. Proteins were visualized using Enhanced Chemiluminescence Western Blotting Substrate (Thermo Scientific Pierce).

Serum hormone analysis

To determine serum hormone levels, 1 to 2 ml of blood was collected from the jugular veins of donor mice before euthanasia, centrifuged to isolate plasma, and stored at −80°C until analyses. The levels of testosterone, FSH, and LH hormones were measured using their respective enzyme-linked immunosorbent assay kits.

Sperm counts and motility analysis

The epididymal caput and cauda were minced and incubated in prewarmed M16 medium (Sigma-Aldrich) at 37°C in air containing 5% CO_2 for 30 min to allow the sperm to swim out. The sperm were then diluted in water and counted using a hemocytometer.

Statistical analysis

All statistical analyses were performed using GraphPad Prism (v7.0). All experiments were repeated at least three times, and data for evaluated parameters were reported as means ± SEM. *P* values were obtained using two-tailed unpaired Student's *t* tests or one-way analysis of variance (ANOVA) followed by Tukey's test ($^{ns}P > 0.05$; $^{*}P < 0.05$; $^{**}P < 0.01$; $^{***}P < 0.001$; $^{****}P < 0.0001$).

Supplementary Materials

This PDF file includes:
Figs. S1 to S8
Legends for tables S1 to S7

Other Supplementary Material for this manuscript includes the following:
Tables S1 to S7

REFERENCES AND NOTES

1. K. Zohni, X. Zhang, S. L. Tan, P. Chan, M. C. Nagano, The efficiency of male fertility restoration is dependent on the recovery kinetics of spermatogonial stem cells after cytotoxic treatment with busulfan in mice. *Hum. Reprod.* **27**, 44–53 (2012).
2. B. Y. Ryu, K. E. Orwig, J. M. Oatley, M. R. Avarbock, R. L. Brinster, Effects of aging and niche microenvironment on spermatogonial stem cell self-renewal. *Stem Cells* **24**, 1505–1511 (2006).
3. M. Sakai, K. Masaki, S. Aiba, M. Tone, S. Takashima, Expression dynamics of self-renewal factors for spermatogonial stem cells in the mouse testis. *J. Reprod. Dev.* **64**, 267–275 (2018).
4. V. Sorrentino, M. Giorgi, R. Geremia, P. Besmer, P. Rossi, Expression of the c-kit proto-oncogene in the murine male germ cells. *Oncogene* **6**, 149–151 (1991).
5. L. Y. Chen, W. D. Willis, E. M. Eddy, Targeting the Gdnf gene in peritubular myoid cells disrupts undifferentiated spermatogonial cell development. *Proc. Natl. Acad. Sci. U.S.A.* **113**, 1829–1834 (2016).
6. B. P. Mullaney, M. K. Skinner, Basic fibroblast growth factor (bFGF) gene expression and protein production during pubertal development of the seminiferous tubule: Follicle-stimulating hormone-induced Sertoli cell bFGF expression. *Endocrinology* **131**, 2928–2934 (1992).
7. Y. Nakamura, D. J. Jörg, Y. Kon, B. D. Simons, S. Yoshida, Transient suppression of transplanted spermatogonial stem cell differentiation restores fertility in mice. *Cell Stem Cell* **28**, 1443–1456.e7 (2021).
8. C. D. Green, Q. Ma, G. L. Manske, A. N. Shami, X. Zheng, S. Marini, L. Moritz, C. Sultan, S. J. Gurczynski, B. B. Moore, M. D. Tallquist, J. Z. Li, S. S. Hammoud, A comprehensive roadmap of murine spermatogenesis defined by single-cell RNA-seq. *Dev. Cell* **46**, 651–667.e10 (2018).
9. K. Tan, H. W. Song, M. F. Wilkinson, Single-cell RNAseq analysis of testicular germ and somatic cell development during the perinatal period. *Development* **147**, dev183251 (2020).
10. M. Wang, X. Liu, G. Chang, Y. Chen, G. An, L. Yan, S. Gao, Y. Xu, Y. Cui, J. Dong, Y. Chen, X. Fan, Y. Hu, K. Song, X. Zhu, Y. Gao, Z. Yao, S. Bian, Y. Hou, J. Lu, R. Wang, Y. Fan, Y. Lian, W. Tang, Y. Wang, J. Liu, L. Zhao, L. Wang, Z. Liu, R. Yuan, Y. Shi, B. Hu, X. Ren, F. Tang, X. Y. Zhao,

J. Qiao, Single-cell rna sequencing analysis reveals sequential cell fate transition during human spermatogenesis. *Cell Stem Cell* **23**, 599–614.e4 (2018).
11. I. Stévant, F. Kühne, A. Greenfield, M. C. Chaboissier, E. T. Dermitzakis, S. Nef, Dissecting cell lineage specification and sex fate determination in gonadal somatic cells using single-cell transcriptomics. *Cell Rep.* **26**, 3272–3283.e3 (2019).
12. A. Sohni, K. Tan, H. W. Song, D. Burow, D. G. de Rooij, L. Laurent, T. C. Hsieh, R. Rabah, S. S. Hammoud, E. Vicini, M. F. Wilkinson, The neonatal and adult human testis defined at the single-cell level. *Cell Rep.* **26**, 1501–1517.e4 (2019).
13. J. Guo, X. Nie, M. Giebler, H. Mlcochova, Y. Wang, E. J. Grow, R. Kim, M. Tharmalingam, G. Matilionyte, C. Lindskog, D. T. Carrell, R. T. Mitchell, A. Goriely, J. M. Hotaling, B. R. Cairns, The dynamic transcriptional cell atlas of testis development during human puberty. *Cell Stem Cell* **26**, 262–276.e4 (2020).
14. J. Guo, E. J. Grow, C. Yi, H. Mlcochova, G. J. Maher, C. Lindskog, P. J. Murphy, C. L. Wike, D. T. Carrell, A. Goriely, J. M. Hotaling, B. R. Cairns, Chromatin and single-cell RNA-seq profiling reveal dynamic signaling and metabolic transitions during human spermatogonial stem cell development. *Cell Stem Cell* **21**, 533–546.e6 (2017).
15. J. Guo, E. J. Grow, H. Mlcochova, G. J. Maher, C. Lindskog, X. Nie, Y. Guo, Y. Takei, J. Yun, L. Cai, R. Kim, D. T. Carrell, A. Goriely, J. M. Hotaling, B. R. Cairns, The adult human testis transcriptional cell atlas. *Cell Res.* **28**, 1141–1157 (2018).
16. S. Yoshida, Open niche regulation of mouse spermatogenic stem cells. *Dev. Growth Differ.* **60**, 542–552 (2018).
17. Y. Tadokoro, K. Yomogida, H. Ohta, A. Tohda, Y. Nishimune, Homeostatic regulation of germinal stem cell proliferation by the GDNF/FSH pathway. *Mech. Dev.* **113**, 29–39 (2002).
18. S. J. Morrison, N. M. Shah, D. J. Anderson, Regulatory mechanisms in stem cell biology. *Cell* **88**, 287–298 (1997).
19. F. M. Watt, B. L. Hogan, Out of Eden: Stem cells and their niches. *Science* **287**, 1427–1430 (2000).
20. H. Ohta, A. Tohda, Y. Nishimune, Proliferation and differentiation of spermatogonial stem cells in the w/wv mutant mouse testis. *Biol. Reprod.* **69**, 1815–1821 (2003).
21. X. Li, T. Sun, X. Wang, J. Tang, Y. Liu, Restore natural fertility of Kit(w)/Kit(wv) mouse with nonobstructive azoospermia through gene editing on SSCs mediated by CRISPR-Cas9. *Stem Cell Res Ther* **10**, 271 (2019).
22. T. Ogawa, I. Dobrinski, M. R. Avarbock, R. L. Brinster, Transplantation of male germ line stem cells restores fertility in infertile mice. *Nat. Med.* **6**, 29–34 (2000).
23. H. Kubota, M. R. Avarbock, J. A. Schmidt, R. L. Brinster, Spermatogonial stem cells derived from infertile Wv/Wv mice self-renew in vitro and generate progeny following transplantation. *Biol. Reprod.* **81**, 293–301 (2009).
24. H. Kuroda, H. Nakayama, M. Namiki, K. Matsumoto, Y. Nishimune, Y. Kitamura, Differentiation of germ cells in seminiferous tubules transplanted to testes of germ cell-deficient mice of W/Wv and Sl/Sld genotypes. *J. Cell. Physiol.* **139**, 329–334 (1989).
25. N. D. Serra, E. K. Velte, B. A. Niedenberger, O. Kirsanov, C. B. Geyer, Cell-autonomous requirement for mammalian target of rapamycin (Mtor) in spermatogonial proliferation and differentiation in the mouse. *Biol. Reprod.* **96**, 816–828 (2017).
26. J. T. Busada, V. A. Chappell, B. A. Niedenberger, E. P. Kaye, B. D. Keiper, C. A. Hogarth, C. B. Geyer, Retinoic acid regulates Kit translation during spermatogonial differentiation in the mouse. *Dev. Biol.* **397**, 140–149 (2015).
27. J. T. Busada, B. A. Niedenberger, E. K. Velte, B. D. Keiper, C. B. Geyer, Mammalian target of rapamycin complex 1 (mTORC1) is required for mouse spermatogonial differentiation in vivo. *Dev. Biol.* **407**, 90–102 (2015).
28. Z. He, J. Jiang, M. Kokkinaki, N. Golestaneh, M. C. Hofmann, M. Dym, Gdnf upregulates c-Fos transcription via the Ras/Erk1/2 pathway to promote mouse spermatogonial stem cell proliferation. *Stem Cells* **26**, 266–278 (2008).
29. C. C. Ke, Y. H. Lin, Y. Y. Wang, Y. Y. Wu, M. F. Chen, W. C. Ku, H. S. Chiang, T. H. Lai, TBC1D21 potentially interacts with and regulates rap1 during murine spermatogenesis. *Int. J. Mol. Sci.* **19**, 3292 (2018).
30. Z. Niu, H. Mu, H. Zhu, J. Wu, J. Hua, p38 MAPK pathway is essential for self-renewal of mouse male germline stem cells (mGSCs). *Cell Prolif.* **50**, e12314 (2017).
31. H. Kubota, R. L. Brinster, Culture of rodent spermatogonial stem cells, male germline stem cells of the postnatal animal. *Methods Cell Biol.* **86**, 59–84 (2008).
32. P. Saharinen, K. Kerkelä, N. Ekman, M. Marron, N. Brindle, G. M. Lee, H. Augustin, G. Y. Koh, K. Alitalo, Multiple angiopoietin recombinant proteins activate the Tie1 receptor tyrosine kinase and promote its interaction with Tie2. *J. Cell Biol.* **169**, 239–243 (2005).
33. G. Velasco-Loyden, J. Arribas, F. López-Casillas, The shedding of betaglycan is regulated by pervanadate and mediated by membrane type matrix metalloprotease-1. *J. Biol. Chem.* **279**, 7721–7733 (2004).
34. Y. Kitadate, D. J. Jörg, M. Tokue, A. Maruyama, R. Ichikawa, S. Tsuchiya, E. Segi-Nishida, T. Nakagawa, A. Uchida, C. Kimura-Yoshida, S. Mizuno, F. Sugiyama, T. Azami, M. Ema, C. Noda, S. Kobayashi, I. Matsuo, Y. Kanai, T. Nagasawa, Y. Sugimoto, S. Takahashi, B. D. Simons, S. Yoshida, Competition for mitogens regulates spermatogenic stem cell homeostasis in an open niche. *Cell Stem Cell* **24**, 79–92.e6 (2019).
35. K. Hara, T. Nakagawa, H. Enomoto, M. Suzuki, M. Yamamoto, B. D. Simons, S. Yoshida, Mouse spermatogenic stem cells continually interconvert between equipotent singly isolated and syncytial states. *Cell Stem Cell* **14**, 658–672 (2014).
36. A. R. Helsel, Q. E. Yang, M. J. Oatley, T. Lord, F. Sablitzky, J. M. Oatley, ID4 levels dictate the stem cell state in mouse spermatogonia. *Development* **144**, 624–634 (2017).
37. M. Jijiwa, K. Kawai, J. Fukihara, A. Nakamura, M. Hasegawa, C. Suzuki, T. Sato, A. Enomoto, N. Asai, Y. Murakumo, M. Takahashi, GDNF-mediated signaling via RET tyrosine 1062 is essential for maintenance of spermatogonial stem cells. *Genes Cells* **13**, 365–374 (2008).
38. M. Sharma, A. Srivastava, H. E. Fairfield, D. Bergstrom, W. F. Flynn, R. E. Braun, Identification of EOMES-expressing spermatogonial stem cells and their regulation by PLZF. *eLife* **8**, e43352 (2019).
39. G. M. Aloisio, Y. Nakada, H. D. Saatcioglu, C. G. Peña, M. D. Baker, E. D. Tarnawa, J. Mukherjee, H. Manjunath, A. Bugde, A. L. Sengupta, J. F. Amatruda, I. Cuevas, F. K. Hamra, D. H. Castrillon, PAX7 expression defines germline stem cells in the adult testis. *J. Clin. Invest.* **124**, 3929–3944 (2014).
40. A. Sada, A. Suzuki, H. Suzuki, Y. Saga, The RNA-binding protein NANOS2 is required to maintain murine spermatogonial stem cells. *Science* **325**, 1394–1398 (2009).
41. M. Tokue, K. Ikami, S. Mizuno, C. Takagi, A. Miyagi, R. Takada, C. Noda, Y. Kitadate, K. Hara, H. Mizuguchi, T. Sato, M. M. Taketo, F. Sugiyama, T. Ogawa, S. Kobayashi, N. Ueno, S. Takahashi, S. Takada, S. Yoshida, SHISA6 confers resistance to differentiation-promoting Wnt/β-catenin signaling in mouse spermatogenic stem cells. *Stem Cell Rep.* **8**, 561–575 (2017).
42. H. M. La, J. A. Mäkelä, A. L. Chan, F. J. Rossello, C. M. Nefzger, J. M. D. Legrand, M. De Seram, J. M. Polo, R. M. Hobbs, Identification of dynamic undifferentiated cell states within the male germline. *Nat. Commun.* **9**, 2819 (2018).
43. J. M. Oatley, M. R. Avarbock, R. L. Brinster, Glial cell line-derived neurotrophic factor regulation of genes essential for self-renewal of mouse spermatogonial stem cells is dependent on Src family kinase signaling. *J. Biol. Chem.* **282**, 25842–25851 (2007).
44. R. Guo, Z. Yu, J. Guan, Y. Ge, J. Ma, S. Li, S. Wang, S. Xue, D. Han, Stage-specific and tissue-specific expression characteristics of differentially expressed genes during mouse spermatogenesis. *Mol. Reprod. Dev.* **67**, 264–272 (2004).
45. T. Nakagawa, D. J. Jörg, H. Watanabe, S. Mizuno, S. Han, T. Ikeda, Y. Omatsu, K. Nishimura, M. Fujita, S. Takahashi, G. Kondoh, B. D. Simons, S. Yoshida, T. Nagasawa, A multistate stem cell dynamics maintains homeostasis in mouse spermatogenesis. *Cell Rep.* **37**, 109875 (2021).
46. M. Pérez-Crespo, E. Pericuesta, S. Pérez-Cerezales, M. I. Arenas, M. V. Lobo, J. J. Díaz-Gil, A. Gutierrez-Adan, Effect of liver growth factor on both testicular regeneration and recovery of spermatogenesis in busulfan-treated mice. *Reprod. Biol. Endocrinol.* **9**, 21 (2011).
47. D. H. Bhang, B. J. Kim, B. G. Kim, K. Schadler, K. H. Baek, Y. H. Kim, W. Hsiao, B. S. Ding, S. Rafii, M. J. Weiss, S. T. Chou, T. F. Kolon, J. P. Ginsberg, B. Y. Ryu, S. Ryeom, Testicular endothelial cells are a critical population in the germline stem cell niche. *Nat. Commun.* **9**, 4379 (2018).
48. T. DeFalco, S. J. Potter, A. V. Williams, B. Waller, M. J. Kan, B. Capel, Macrophages contribute to the spermatogonial niche in the adult testis. *Cell Rep.* **12**, 1107–1119 (2015).
49. N. Abou Nader, A. Levasseur, X. Zhang, D. Boerboom, M. C. Nagano, A. Boyer, Yes-associated protein expression in germ cells is dispensable for spermatogenesis in mice. *Genesis* **57**, e23330 (2019).
50. Y. Tang, T. Feinberg, E. T. Keller, X. Y. Li, S. J. Weiss, Snail/Slug binding interactions with YAP/TAZ control skeletal stem cell self-renewal and differentiation. *Nat. Cell Biol.* **18**, 917–929 (2016).
51. V. Evdokimova, C. E. Tognon, T. Benatar, W. Yang, K. Krutikov, M. Pollak, P. H. Sorensen, A. Seth, IGFBP7 binds to the IGF-1 receptor and blocks its activation by insulin-like growth factors. *Sci. Signal.* **5**, ra92 (2012).
52. M. Amoyel, K. H. Hillion, S. R. Margolis, E. A. Bach, Somatic stem cell differentiation is regulated by PI3K/Tor signaling in response to local cues. *Development* **143**, 3914–3925 (2016).
53. Y. Wen, H. Yang, J. Wu, A. Wang, X. Chen, S. Hu, Y. Zhang, D. Bai, Z. Jin, COL4A2 in the tissue-specific extracellular matrix plays important role on osteogenic differentiation of periodontal ligament stem cells. *Theranostics* **9**, 4265–4286 (2019).
54. M. A. Sarraj, R. M. Escalona, A. Umbers, H. K. Chua, C. Small, M. Griswold, K. Loveland, J. K. Findlay, K. L. Stenvers, Fetal testis dysgenesis and compromised Leydig cell function in Tgfbr3 (beta glycan) knockout mice. *Biol. Reprod.* **82**, 153–162 (2010).
55. L. Xiang, J. Zheng, M. Zhang, T. Ai, B. Cai, FOXQ1 promotes the osteogenic differentiation of bone mesenchymal stem cells via Wnt/β-catenin signaling by binding with ANXA2. *Stem Cell Res Ther* **11**, 403 (2020).
56. T. Stuart, A. Butler, P. Hoffman, C. Hafemeister, E. Papalexi, W. M. Mauck III, Y. Hao, M. Stoeckius, P. Smibert, R. Satija, Comprehensive integration of single-cell data. *Cell* **177**, 1888–1902.e21 (2019).

57. C. Trapnell, D. Cacchiarelli, J. Grimsby, P. Pokharel, S. Li, M. Morse, N. J. Lennon, K. J. Livak, T. S. Mikkelsen, J. L. Rinn, The dynamics and regulators of cell fate decisions are revealed by pseudotemporal ordering of single cells. *Nat. Biotechnol.* **32**, 381–386 (2014).
58. M. Nagano, M. R. Avarbock, R. L. Brinster, Pattern and kinetics of mouse donor spermatogonial stem cell colonization in recipient testes. *Biol. Reprod.* **60**, 1429–1436 (1999).
59. S. Di Persio, R. Saracino, S. Fera, B. Muciaccia, V. Esposito, C. Boitani, B. P. Berloco, F. Nudo, G. Spadetta, M. Stefanini, D. G. de Rooij, E. Vicini, Spermatogonial kinetics in humans. *Development* **144**, 3430–3439 (2017).
60. K. Zheng, X. Wu, K. H. Kaestner, P. J. Wang, The pluripotency factor LIN28 marks undifferentiated spermatogonia in mouse. *BMC Dev. Biol.* **9**, 38 (2009).
61. T. Nakagawa, M. Sharma, Y. Nabeshima, R. E. Braun, S. Yoshida, Functional hierarchy and reversibility within the murine spermatogenic stem cell compartment. *Science* **328**, 62–67 (2010).

Acknowledgments
Funding: This study was supported by the following grants: National Key Research and Development Program of China (2022YFA0806302, 2018YFC1003500, 2019YFA0801800, and 2019YFA0802600), Chinese Academy of Medical Sciences (CAMS) Innovation Fund for Medical Sciences (2021-1-I2M-019 and 2017-I2M-3-009), National Natural Science Foundation of China (92268111, 81672472, 31970794, 32000586, 31725013, and 32200646), and State Key Laboratory Special fund from the Ministry of Science (2060204). **Author contributions:** W.S., C.J., J.Y., and K.L. conceived and designed the study. C.J. and Z.W. performed most of the experiments and analyzed the data with the help of P.L. and J.T. T.J., Y.Li., J.O., D.Z., M.L., X.M., J.L., M.H., Y.Lu., and K.L. provided additional experimental support. S.C., X.W., and J.S. performed the SNP analysis. J.Y., N.Z., F.S., Y.M., S.M., and L.W. provided critical suggestions for manuscript preparation. W.S. and C.J. wrote the manuscript with help from all authors. **Competing interests:** The authors declare that they have no competing interests. **Data and materials availability:** All data needed to evaluate the conclusions in the paper are present in the paper and/or the Supplementary Materials. The scRNA-seq data were uploaded to Gene Expression Omnibus (GEO) with the accession code GSE164787. The GEO accession codes for previously published human datasets used in this study are GSE108885, GSE145467, GSE45885, GSE124263, and GSE112013. All R packages that were used are available online, as described in Materials and Methods and the Supplementary Materials. MSigDB (v.7.0) used in this study is available at www.gsea-msigdb.org/gsea/msigdb.

Submitted 18 April 2022
Accepted 3 July 2023
Published 4 August 2023
10.1126/sciadv.abq3173

ScienceAdvances

Decoding the spermatogonial stem cell niche under physiological and recovery conditions in adult mice and humans

Cheng Jin, Zhipeng Wang, Pengyu Li, Jielin Tang, Tao Jiao, Yiran Li, Jinhuan Ou, Dingfeng Zou, Mengzhen Li, Xinyu Mang, Jun Liu, Yanni Ma, Xiaolong Wu, Jie Shi, Shitao Chen, Manman He, Yan Lu, Ning Zhang, Shiying Miao, Fei Sun, Linfang Wang, Kai Li, Jia Yu, and Wei Song

Sci. Adv., **9** (31), eabq3173.
DOI: 10.1126/sciadv.abq3173

Science Advances (ISSN) is published by the American Association for the Advancement of Science. 1200 New York Avenue NW, Washington, DC 20005. The title *Science Advances* is a registered trademark of AAAS.